Cellular/Molecular

Synaptic Zn^{2+} Inhibits Neurotransmitter Release by Promoting Endocannabinoid Synthesis

Tamara Perez-Rosello,[1] **Charles T. Anderson,**[1] **Francisco J. Schopfer,**[2] **Yanjun Zhao,**[1] **David Gilad,**[4] **Sonia R. Salvatore,**[2] **Bruce A. Freeman,**[2] **Michal Hershfinkel,**[4] **Elias Aizenman,**[3,4] **and Thanos Tzounopoulos**[1,3]

Departments of [1]Otolaryngology, [2]Pharmacology and Chemical Biology, and [3]Neurobiology, University of Pittsburgh School of Medicine, Pittsburgh, Pennsylvania 15261, and [4]Department of Morphology, Ben-Gurion University, Faculty of Health Sciences, Beer-Sheva 84015, Israel

Although it is well established that many glutamatergic neurons sequester Zn^{2+} within their synaptic vesicles, the physiological significance of synaptic Zn^{2+} remains poorly understood. In experiments performed in a Zn^{2+}-enriched auditory brainstem nucleus—the dorsal cochlear nucleus—we discovered that synaptic Zn^{2+} and GPR39, a putative metabotropic Zn^{2+}-sensing receptor (mZnR), are necessary for triggering the synthesis of the endocannabinoid 2-arachidonoylglycerol (2-AG). The postsynaptic production of 2-AG, in turn, inhibits presynaptic probability of neurotransmitter release, thus shaping synaptic strength and short-term synaptic plasticity. Zn^{2+}-induced inhibition of transmitter release is absent in mutant mice that lack either vesicular Zn^{2+} or the mZnR. Moreover, mass spectrometry measurements of 2-AG levels reveal that Zn^{2+}-mediated initiation of 2-AG synthesis is absent in mice lacking the mZnR. We reveal a previously unknown action of synaptic Zn^{2+}: synaptic Zn^{2+} inhibits glutamate release by promoting 2-AG synthesis.

Introduction

Zn^{2+} is, after iron, the second most abundant trace element in humans. As an essential element for living organisms, Zn^{2+} plays a catalytic and structural role in many enzymes and regulatory proteins (Vallee, 1988). Since the surprising discovery that Zn^{2+} is present in large amounts within synaptic vesicles in many areas of the brain (Maske, 1955), numerous studies have investigated the possible roles of this metal on synaptic function. These studies have revealed that synaptic Zn^{2+}, as an allosteric modulator, inhibits $GABA_A$, NMDA, and kainate receptors (Paoletti et al., 1997; Vogt et al., 2000; Ruiz et al., 2004; Mott et al., 2008; Nozaki et al., 2011; Veran et al., 2012), while potentiating glycine receptors (Hirzel et al., 2006). Moreover, synaptic Zn^{2+}, as a trigger of signaling pathways, is thought to be required for mossy fiber long-term potentiation (LTP) via presynaptic and postsynaptic mechanisms (Huang et al., 2008; Pan et al., 2011); however, these results are not consistent with other studies suggesting that Zn^{2+} signaling does not affect mossy fiber LTP (Vogt et al., 2000; Lavoie et al., 2011). Indeed, the establishment of specific presynaptic or postsynaptic pathways of Zn^{2+}-mediated signaling and

their physiological role on neuronal processing remain poorly understood.

The uniquely high concentrations of synaptic Zn^{2+} in the dorsal cochlear nucleus (DCN) (Frederickson et al., 1988), an auditory brainstem nucleus with well characterized circuitry and cellular mechanisms modulating synaptic transmission (Oertel and Young, 2004; Bender and Trussell, 2011), provide an attractive model for studying the role of synaptically released Zn^{2+} in regulating synaptic transmission. DCN principal neurons receive Zn^{2+}-rich excitatory parallel fiber inputs in their apical dendrites, yet the physiological consequences of synaptic Zn^{2+} release in this circuit are completely unknown. Here, we report an unexpected Zn^{2+}-mediated signaling pathway wherein synaptic Zn^{2+} reduces presynaptic glutamate release by triggering endocannabinoid synthesis. Our results reveal a previously unknown Zn^{2+}-mediated signaling pathway that establishes a role of synaptic Zn^{2+} release in regulating neurotransmission.

Materials and Methods

Slice preparation

Experiments were conducted according to the methods approved by the Institutional Animal Care and Use Committee of the University of Pittsburgh. Coronal brainstem slices were prepared from either sex ICR, mZnR wild-type (mZnR WT) and knock-out (mZnR KO), and ZnT3 wild-type (ZnT3 WT) and knock-out (ZnT3 KO) mice (P17–P25). The preparation of coronal slices containing DCN has been described in detail (Tzounopoulos et al., 2004).

Electrophysiology

In vitro *recordings*. Whole-cell voltage-clamp and current-clamp recordings were obtained from visually identified fusiform cells at a temperature of 31–33°C. Fusiform cells were identified on the basis of morphological and electrophysiological criteria (Tzounopoulos et al., 2004). For DCN recordings the external solution contained the following (in mM): 130 NaCl, 3 KCl, 2.4 $CaCl_2$, 1.3 $MgSO_4$, 21 $NaHCO_3$, 3.5 HEPES, and 10 glucose; saturated with 95% O_2/5% CO_2.

For EPSC recordings fusiform cells were voltage clamped at -70 mV using pipettes with a K^+-based internal solution of the following (in mM): 113 K-gluconate, 1.5 $MgCl_2$, 14 Tris-phosphocreatine, 9 HEPES, 0.1 EGTA, 4 Na-ATP, 0.3 Tris-GTP, and 1 sucrose. All the internal solutions were adjusted to pH 7.3, $\sim$285 mOsmol. Voltage-clamp experiments were not included if the series and/or input resistance changed >20% during the recording. EPSCs in fusiform cells were evoked by stimulating parallel fiber tracts (0.2 Hz) in the presence of SR95531 ($GABA_A$ receptor antagonist, 20 μM) and strychnine (glycine receptor antagonist, 0.5 μM). Fiber tracts were stimulated with voltage pulses (100 μs, 10–30 V). To measure the time course of pharmacological manipulations, EPSC peak amplitude was measured and averaged every minute, then normalized to baseline. To ensure washout of bath-applied Zn^{2+} we perfused the slices at a rate of 6 ml/min. Synaptic Zn^{2+} release was induced by electrical stimulation of the parallel fibers using a protocol consisting of 100 pulses at 100 Hz and 30 pulses at 30 Hz. For depolarization-induced suppression of excitation (DSE) experiments, baseline EPSCs were acquired at a stimulation frequency of 0.67 Hz, followed by a depolarization of 5 s to 10 mV delivered to the postsynaptic cell. EPSC amplitude was measured and averaged from 10 sweeps in each cell and normalized to the average value before depolarization. DSE is reported as a percentage of average EPSCs 1–3 s after depolarization versus before depolarization. Electrophysiological data were acquired and analyzed using pClamp (Molecular Devices), IGOR Pro (Wavemetrics), and GraphPad Prism (GraphPad Software). All means are reported $\pm$ SEM. Statistical comparisons were made using ANOVA, and paired and unpaired two-tailed Student's t tests. Statistical significance was based on p values <0.05. All means are reported $\pm$ SEM.

mEPSCs recordings. mEPSCs were recorded at a holding potential of -70 mV in the presence of tetrodotoxin (TTX; 0.5 μM), SR95531 (20 μM), and strychnine (0.5 μM). The intracellular solution contained the following (in mM): 128 $CsMeSO_3$, 10 HEPES, 1 EGTA, 4 $MgCl_2$, 4 ATP, 0.3 GTP, 10 phosphocreatine, 1 Cs-EGTA, 3 ascorbate, and 0.5 QX-314 (a blocker of voltage-activated Na^+ channels). Ten second blocks of mEPSCs were acquired at a sample rate of 50 kHz and low-pass filtered at 10 kHz. Negative-voltage pulses (5 mV, 50 ms) were delivered every 10 s to monitor input and access resistance; mEPSC experiments were not included if the series and/or input resistance changed >20% during the recording. mEPSCs were detected and analyzed using Mini Analysis software (Synaptosoft) with amplitude and area threshold set at 3 root mean square noise level. All events were verified by visual inspection. Amplitude values were obtained by subtracting the average baseline from the amplitude at the local maximum during the event. Rise times were measured as time difference between 10 and 90% of the peak amplitude. Decay time was calculated as a time that took the event to decay to 37% of the peak amplitude.

Fluorescence imaging

For Ca^{2+} imaging, slices were loaded with fura-2 AM (25 μM, TEFLabs) for 20 min at room temperature, in the presence of 0.02% pluronic acid, and then washed in artificial CSF (ACSF) for at least 20 min (Besser et al., 2009). For extracellular Zn^{2+} imaging, Newport Green (2 μM) was added to the slice. Slices were then loaded in a microscope chamber and perfused with PO_4-free ACSF to avoid Zn^{2+} precipitation (Chorin et al., 2011). Fluorescent imaging measurements were acquired every 3 s (Imaging Workbench 4, INDEC BioSystems and polychrome monochromator, TILL Photonics) using a 10$\times$ objective (Olympus BX51) with 4 $\times$ 4 binning of the image (SensiCam; PCO). Regions of interest (ROI) were chosen throughout the DCN molecular layer that was not covered by the stimulating electrode, and traces from four ROIs were averaged for each slice. Cell bodies are surrounded by our selected ROIs, thus, the observed fura-2 fluorescence changes mostly represent the result of Ca^{2+} rises in neuronal cell bodies. Fura-2 fluorescence signals are represented as a ratio of the signal obtained using excitation of 340 nm/380 nm wavelengths and a 510 nm emission bandpass filter (Chroma Technology). Newport Green fluorescent signals were normalized to the initial fluorescent level (F_0) and the signal is represented as F/F_0. Bar graphs represent the averaged difference in the fluorescent signal averaged over n slices as indicated. The stimulating electrode was placed on the molecular

layer of the DCN and a train of 100 pulses at 100 Hz was applied (Master-8 stimulator unit; A.M.P.I.). When required, the initial baseline was used to calculate a linear regression curve that was subtracted from the trace.

2-Arachidonoylglycerol quantification

A modified isotopic dilution liquid chromatography/tandem mass spectrometry (LC/MS/MS) method (Zhang et al., 2010) was used to determine 2-arachidonoylglycerol (2-AG) in DCN slices. DCN slices were incubated at 37°C for $\sim$30 min to allow the tissue to recover after the cutting procedure (similar to electrophysiological experiments). 2-AG concentrations were measured in control samples and samples exposed to Zn^{2+} (100 μM, 5 min) in the presence or absence of U73122 (5 μM). In experiments in which U73122 was used, slices were pretreated with this drug or vehicle for 30 min. After this pretreatment, both control and treated slices were transferred to a chamber with either normal solution or Zn^{2+}-containing solution for 5 min (U73122 was also present during the 5 min treatment). Samples were then immediately flash-frozen and stored in liquid nitrogen. The tissues were later thawed and homogenized in 20 μl of H_2O with 0.02% trifluoroacetic acid and 2 μl aliquots were used for protein concentration determinations using the Bradford method. Then, 180 μl of cold acetonitrile was added to the samples previously spiked with 9 pmol 2-AG-d8 internal standard and followed by homogenization. The samples were centrifuged at 14,000 g for 10 min at 4°C and the supernatant transferred into vials. Brain homogenates at a 5 mg tissue/ml were used to perform quantification quality controls by spiking samples with internal standard and 300 pmol of 1-AG and 2-AG per milligrams of tissue. Samples were thawed and homogenized in the presence of deuterated 2-AG internal standard, thus controlling for any loss during sample work-up. The internal standard corrects for losses due to degradation, extraction efficiency, binding to silica present in the glass tubes, gas phase equilibrium, and ionization efficiencies. The concentration of 2-AG was normalized to amounts of DCN protein to avoid the errors introduced by handling small amounts of tissue per DCN slice (typically <1 mg).

Standard curve preparation. A calibration curve was prepared by serial stock dilutions of 2-AG and 1-AG. Three independent standard curves were prepared and the limit of detection (3 $\times$ signal-to-noise ratio) and limit of quantification (LOQ) concentrations calculated (LOQ was defined as the lowest concentration displaying a relative SD percentage lower than 15).

LC. The chromatography was performed on a Shimadzu SIL-20A HPLC equipped with a degasser, autosampler, and column oven (set at 37°C) on a 2.0 mm ID, 150 mm long, 3 μm C-18 Luna column (Phenomenex). The solvent system used consisted of 0.1% acetic acid in H_2O and 0.1% acetic acid in acetonitrile.

MS. The flow after the column was split and one-third was sent to a triple quadrupole for quantification purposes and two-thirds was diverted into an LTQ Velos Orbitrap for high MS resolution ion and product ion determinations. The quantification of 1-AG and 2-AG was performed in positive ion mode using a 4000 QTrap triple quadrupole (Applied Biosystems). The following transitions were optimized and used for quantification of 1-AG and 2-AG (m/z 379 $\rightarrow$ 287) and 2-AG-d8 (m/z 387 $\rightarrow$ 295) using a collision energy of 15, a declustering potential of 50 V, an entrance potential of 8 V, and a collision cell exit potential of 15 V. High-resolution spectra and accurate mass determinations (at a resolving power of 10,000) were obtained in samples and standards for 2-AG and 1-AG and its product ions.

Experiments with KO mice

Imaging and biochemical experiments were blinded (see Figs. 4, 8). Electrophysiological experiments were partially blinded: initial experiments were not blinded (approximately half n), but all subsequent experiments were blinded (see Figs. 6, 11, 12). As we did not observe any differences in the two datasets, we have included all these experiments.

Drugs and KO mice

SR95531, NBQX disodium salt, QX-314, AM251, TTX, and WIN55, 212–2 mesylate (WIN), were purchased from Ascent Scientific. $ZnCl_2$, strychnine, BAPTA, GDP-β-S, tricine, and tetrahydrolipstatin (THL)
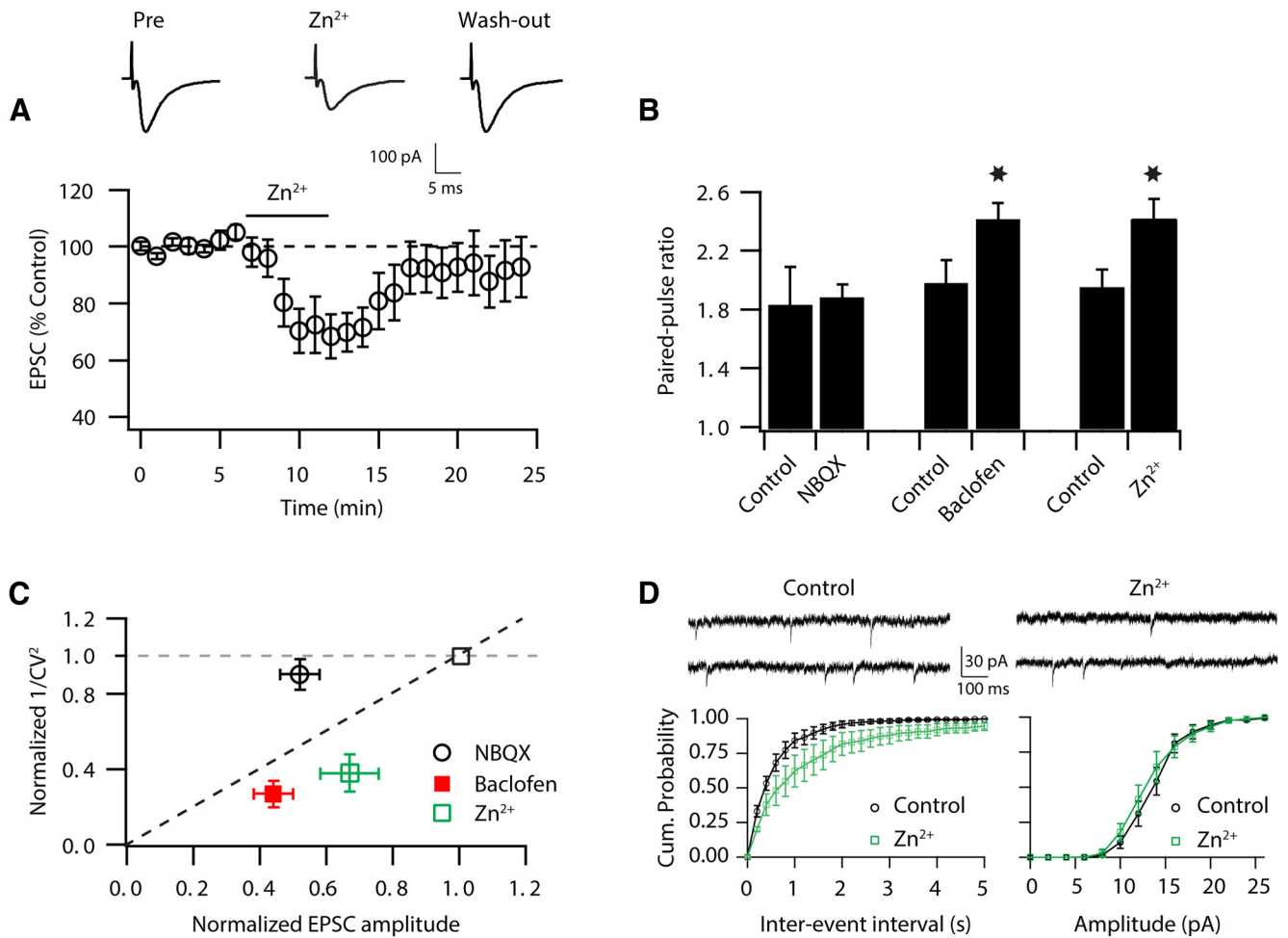
Figure 1. Zn^{2+} reduces synaptic strength by lowering Pr. **A**, Time course of EPSC peak amplitude reversible depression by 100 μM, 5 min Zn^{2+} application. (During Zn^{2+} application: 67.9 ± 9.0% of baseline, $n = 7$, $p < 0.01$; after Zn^{2+} washout: 94.5 ± 9.5% of baseline, $n = 7$, $p = 0.7$). Top, Representative averaged traces of EPSCs before (pre), during Zn^{2+}, and after removal of Zn^{2+} (washout). **B**, PPR (20 ms interstimulus interval) is increased after Zn^{2+} application (PPR: baseline: 1.96 ± 0.11; after Zn^{2+}: 2.42 ± 0.13; $n = 7$, $p < 0.01$). **C**, Zn^{2+}-induced EPSC depression is associated with a decrease in Pr. 1/CV^2 is decreased after Zn^{2+} (1/CV^2 in Zn^{2+}: 0.38 ± 0.1% of baseline, $n = 7$, $p < 0.01$). Effect of baclofen (2–5 μM) on PPR and 1/CV^2 (PPR: baseline: 2.00 ± 0.15; after baclofen: 2.42 ± 0.10; $n = 6$, $p < 0.01$; 1/CV^2 in baclofen: 0.27 ± 0.07% of baseline, $n = 6$, $p < 0.01$). Effect of NBQX (0.5 μM) on PPR and 1/CV^2 (PPR: baseline: 1.84 ± 0.25; after NBQX: 1.89 ± 0.08; $n = 6$, $p = 0.47$; 1/CV^2 in NBQX: 0.90 ± 0.08% of baseline, $n = 8$, $p = 0.55$). **D**, Cumulative probability plot of mEPSC frequencies shows that Zn^{2+} application decreased frequencies (left). Cumulative probability plot of mEPSC amplitudes shows Zn^{2+} application did not affect amplitudes (right). Top, Sample traces of mEPSCs before and after Zn^{2+} application (mean mEPSC frequency: baseline: 1.89 ± 0.3 Hz; after Zn^{2+}: 1.22 ± 0.5 Hz; $n = 4$, $p < 0.05$ paired t test; mean mEPSC amplitude: baseline: 13.79 ± 0.81 pA; after Zn^{2+}: 13.35 ± 0.94 pA; $n = 4$, $p > 0.12$ paired t test). Summary data represent mean ± SEM. Asterisks indicate statistically significant differences, $p < 0.05$.

were purchased from Sigma-Aldrich. The 2-AG, 1-AG, and ^{2}H$_8$ 2-AG standards were purchased from Cayman Chemical. U73122 was purchased from Tocris Cookson. Fura-2 AM and Newport Green were purchased from TEFLabs and Invitrogen, respectively. GPR39/mZnR KO mice were kindly provided by D. Moechars from Janssen, Pharmaceutical Companies of Johnson & Johnson. ZnT3 KO mice were purchased from The Jackson Laboratory.

Results

Zn^{2+} decreases probability of release via activation of endocannabinoid signaling

To investigate the effects of Zn^{2+} on parallel fiber EPSC strength, we obtained whole-cell recordings from DCN principal neurons (fusiform cells). Bath application of Zn^{2+} (100 μM, 5 min) significantly decreased EPSC amplitude (Fig. 1A). The inhibitory effect of Zn^{2+} on EPSC strength was reversed upon Zn^{2+} removal, suggesting that extracellular Zn^{2+} mediates a short-lasting decrease in synaptic strength (Fig. 1A). The observed Zn^{2+}-induced decrease in synaptic strength is due to presynaptic and/or postsynaptic mechanisms. To investigate whether the ef-

fects of Zn^{2+} on synaptic strength are mediated by presynaptic mechanisms, we used two assays that are sensitive to changes in presynaptic neurotransmitter release (Pr): paired-pulse ratio (PPR) and coefficient of variation (CV) analysis (Faber and Korn, 1991; Tsien and Malinow, 1991). Paired-pulse facilitation, an increased second response to two stimuli applied in rapid succession, is thought to reflect an increase in Pr. The CV is the SD of the EPSC amplitudes normalized to the mean amplitude and varies oppositely with quantal content; the inverse square, 1/CV^2, is directly proportional to quantal content (quantal content = n p, where n = number of release sites and p = Pr). Application of Zn^{2+} increased PPR and decreased 1/CV^2, both of which indicate a decrease in Pr (Fig. 1B,C). Baclofen (2–5 μM), which is known to inhibit synaptic strength via a presynaptic mechanism (Dutar and Nicoll, 1988), caused a similar increase in PPR and a similar reduction in 1/CV^2, indicating that PPR and CV assays are highly sensitive to changes in Pr (Fig. 1B,C). Conversely, 0.5 μM 2,3-dihydroxy-6-nitro-7-sulfamoyl-benzo[f]quinoxaline-2,3-dione (NBQX), which reduces synaptic strength by partially

blocking postsynaptic glutamate receptors, left PPR and $1/CV^2$ unaffected, thus confirming that PPR and CV assays are not sensitive to changes in synaptic strength that are mediated by postsynaptic manipulations (Fig. 1B,C). Consistent with these results, application of Zn^{2+} decreased miniature EPSC (mEPSC) frequency without affecting mEPSC amplitude (Fig. 1D). Together, these findings show that the Zn^{2+}-induced EPSC depression is mediated by a decrease in Pr.

Given the role of endocannabinoid retrograde signaling in determining the Pr of DCN parallel fiber synapses (Tzounopoulos et al., 2007; Tzounopoulos and Kraus, 2009; Sedlacek et al., 2011; Zhao and Tzounopoulos, 2011; Zhao et al., 2011), we tested whether endocannabinoids are involved in Zn^{2+}-mediated modulation of Pr. We found that the specific cannabinoid receptor 1 (CB1R) antagonist AM-251 (1 μM) prevented Zn^{2+}-mediated EPSC depression and the concomitant changes in PPR and $1/CV^2$ (Fig. 2A–C). Bath application of AM-251 (1 μM) did not affect baseline synaptic transmission, indicating lack of tonic activation of CB1Rs and lack of tonic endocannabinoid signaling in modulating baseline Pr (Fig. 2D). These results suggest that Zn^{2+}-dependent endocannabinoid signaling mediates Pr reduction, thus revealing an unexpected link between Zn^{2+} and endocannabinoid signaling.

Endocannabinoid modulation of Pr has both postsynaptic (endocannabinoid synthesis and release) and presynaptic (activation of cannabinoid receptors, CB1Rs) components (Alger, 2012). Therefore, we investigated whether Zn^{2+}-dependent modulation of Pr is mediated through direct presynaptic activation or allosteric modulation of CB1Rs, or through initiation of a postsynaptic signaling cascade leading to endocannabinoid synthesis and release. Intracellular application of the calcium chelator BAPTA (10 mM) in fusiform cells blocked Zn^{2+}-induced depression of EPSCs and the concomitant changes in PPR and $1/CV^2$, indicating that an increase in postsynaptic Ca^{2+} is necessary for Zn^{2+}-mediated modulation of Pr (Fig. 3A–C). While BAPTA also chelates intracellular Zn^{2+} (Hyrc et al., 2000), subsequent experiments using the extracellular Zn^{2+} chelator tricine (Figs. 4, 9, 11) are consistent with a lack of dependence of our proposed mechanism on an intracellular Zn^{2+} increase. In addition, loading fusiform cells with GDP-β-S (0.5 mM), a nonhydrolyzable analog of GDP, blocked the effects of Zn^{2+} on EPSC amplitude, PPR, and $1/CV^2$, suggesting that postsynaptic activation of G-protein-coupled receptors (GPCRs) mediate Zn^{2+}-induced activation of endocannabinoid signaling (Fig. 3A–C; see also figure legend for control experiments on the lack of effects on GDP-β-S on baseline synaptic transmission). Given that endocannabinoid synthesis from the postsynaptic neuron can be induced by elevations in intracellular Ca^{2+}, by activation of
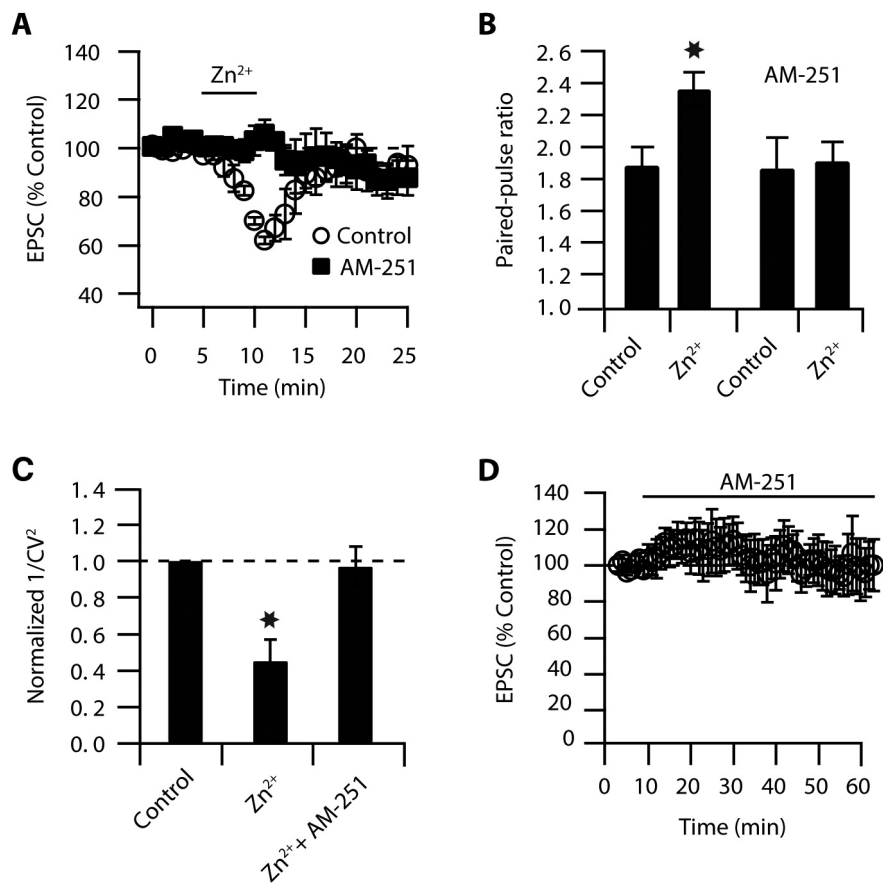
Figure 2. Zn^{2+}-induced decrease in Pr is mediated by endocannabinoid signaling. **A**, Zn^{2+}-induced EPSC depression is blocked by 1 μM AM-251 (EPSC amplitude in control: 66.4 ± 4.8% of baseline, $n = 8$, $p < 0.01$; in AM-251: 91.4 ± 7% of baseline, $n = 6$, $p = 0.3$). **B**, PPR (20 ms interstimulus interval) is increased after Zn^{2+} application in control conditions, but this increase is blocked in the presence of AM-251 (PPR in control: baseline: 1.88 ± 0.12; after Zn^{2+}: 2.36 ± 0.11, $n = 8$, $p < 0.01$; PPR baseline in AM-251: 1.86 ± 0.2; after Zn^{2+}: 1.91 ± 0.12; $n = 6$; $p = 0.19$. **C**, $1/CV^2$ is decreased after Zn^{2+} application in control conditions, but this decrease is blocked in the presence of AM-251 ($1/CV^2$ in Zn^{2+}: 0.45 ± 0.12%, $n = 8$, $p < 0.01$; $1/CV^2$ in Zn^{2+} + AM-251: 0.97 ± 0.11% of baseline, $n = 6$, $p = 0.78$). **D**, Time course of baseline EPSC amplitude before and after application of AM-251 (EPSC amplitude after AM-251 application: 107.6 ± 10.2% of baseline, $n = 5$, $p = 0.34$). Summary data represent mean ± SEM. Asterisks indicate statistically significant differences, $p < 0.05$.

GPCRs, or by concerted activation of GPCRs and elevations in intracellular Ca^{2+} (Wilson and Nicoll, 2001; Kim et al., 2002; Zhao and Tzounopoulos, 2011), our results indicate that Zn^{2+} likely promotes endocannabinoid production through a postsynaptic activation of GPCRs and a rise in intracellular Ca^{2+}.

Zn^{2+}-induced decrease in Pr is mediated by a mZnR-dependent increase of 2-AG synthesis

Since endocannabinoid production is tightly linked to G_q-coupled receptors in the DCN (Zhao and Tzounopoulos, 2011), and because the previously orphan G_q-coupled receptor 39 (GPR39) has emerged as a putative metabotropic Zn^{2+}-sensing receptor (mZnR) (Besser et al., 2009), we evaluated whether mZnR activation is involved in the Zn^{2+}-triggered promotion of endocannabinoid production in the DCN. As activation of mZnRs is thought to lead to Zn^{2+}-mediated increases in intracellular Ca^{2+} in the hippocampus and in cortical neurons (Besser et al., 2009; Saadi et al., 2011; but see Evstratova and Toth, 2011), we determined whether synaptically released Zn^{2+} leads to an mZnR-mediated increase in intracellular Ca^{2+} in the DCN. We measured intracellular Ca^{2+} responses in the molecular layer of DCN slices from WT and from genetically modified mice lacking GPR39 (Moechars et al., 2006) (mZnR KO mice). While parallel
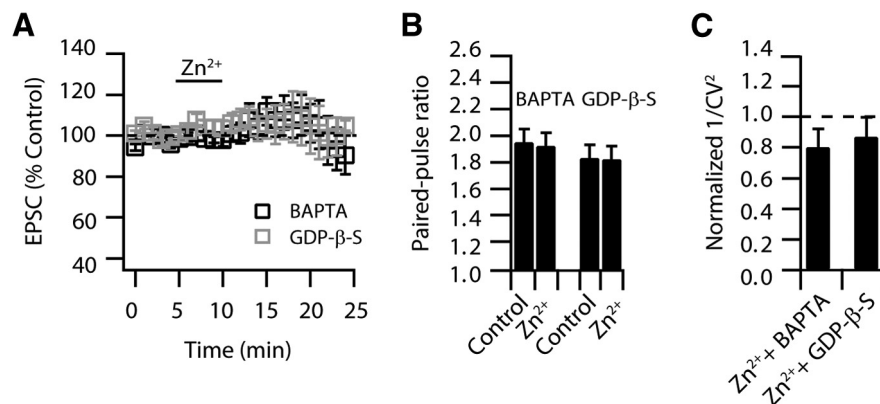
A **B** **C**

Figure 3. Zn^{2+}-induced decrease in Pr requires rises in postsynaptic Ca^{2+} and postsynaptic activation of a GPCR pathway. **A**, Zn^{2+}-induced EPSC depression is blocked by 10 mM intracellular BAPTA or 0.5 mM intracellular GDP-β-S (BAPTA: EPSC amplitude: 99.9 ± 8.5% of baseline, $n = 5$, $p = 0.3$; GDP-β-S: EPSC amplitude: 105.87 ± 4.39% of baseline, $n = 7$, $p = 0.38$). Our previous studies have shown that GDP-β-S does not affect parallel fiber EPSCs in fusiform cells; yet, application of GDP-β-S decreases the input resistance of fusiform cells (Zhao and Tzounopoulos, 2011). Thus, to avoid possible complications in the interpretation of our findings due to changes in input resistance and to allow diffusion of GDP-β-S in fusiform cells, we investigated the effect of GDP-β-S on Zn^{2+}-mediated modulation of Pr after the GDP-β-S-mediated effect on input resistance reached a steady state: Zn^{2+} application took place ~30 min after break-in of the cell. **B**, PPR (20 ms interstimulus interval) was not increased after Zn^{2+} application in the presence of BAPTA and GDP-β-S (BAPTA PPR: baseline: 1.95 ± 0.1; PPR after Zn^{2+}: 1.92 ± 0.1; $n = 5$; $p = 0.49$; GDP-β-S: PPR baseline: 1.83 ± 0.1; PPR after Zn^{2+}: 1.82 ± 0.1; $n = 7$; $p = 0.8$). **C**, $1/CV^2$ was not decreased after Zn^{2+} application in the presence of BAPTA and GDP-β-S (BAPTA: $1/CV^2$: 0.8 ± 0.12% of baseline, $n = 5$, $p = 0.61$; GDP-β-S: $1/CV^2$: 0.87 ± 0.13% of baseline, $n = 7$, $p = 0.78$). Summary data represent mean ± SEM.

fiber stimulation (100 Hz, 1 s) caused robust intracellular Ca^{2+} responses in slices from mZnR WT mice, measurements from littermate mZnR KO mice displayed significantly reduced Ca^{2+} responses (Fig. 4A). To determine whether reduced Ca^{2+} responses in mZnR KO mice are due to the lack of Zn^{2+}-triggered, mZnR-mediated signaling, we measured the sensitivity of the Ca^{2+} responses to tricine: an extracellular Zn^{2+} chelator (Paoletti et al., 2009). Application of 10 mM tricine reduced Ca^{2+} responses in WT mice and left Ca^{2+} responses unaffected in mZnR KO mice; tricine also reduced Ca^{2+} responses in WT mice to levels similar to those observed in mZnR KO mice (Fig. 4A). Because tricine only reduces Ca^{2+} responses in WT mice, but not in KO mice, we conclude that the observed differences in Ca^{2+} responses are due to Zn^{2+}-mediated, mZnR-dependent signaling.

To further support that vesicular Zn^{2+} triggers Zn^{2+}-mediated signaling via mZnR, we used a mouse genetic model lacking the transporter that loads Zn^{2+} into synaptic vesicles (ZnT3 KO) mice (Cole et al., 1999). ZnT3 KO mice lack vesicular Zn^{2+} staining and vesicular Zn^{2+} release (Cole et al., 1999; Qian and Noebels, 2005; Chorin et al., 2011). As expected, while ZnT3 WT mice displayed DCN vesicular Zn^{2+} release after parallel fiber stimulation, DCN vesicular Zn^{2+} release was undetectable in ZnT3 KO mice (Fig. 4B,C). In response to parallel fiber stimulation, ZnT3 KO mice displayed reduced Ca^{2+} responses when compared with WT mice; in addition, tricine did not affect Ca^{2+} responses in ZnT3 KO mice (Fig. 4A). These results indicate that a significant proportion of the Ca^{2+} response following stimulation of the parallel fibers requires both vesicular Zn^{2+} and the mZnR. While fura-2 can also detect changes in intracellular Zn^{2+}, previous studies have established that activation of mZnRs by extracellular Zn^{2+} leads to a phospholipase C (PLC)-dependent increase in intracellular Ca^{2+} that is not associated with Zn^{2+} influx (Besser et al., 2009; Chorin et al., 2011; Saadi et al., 2012). Finally, mZnR KO mice displayed normal DCN vesicular Zn^{2+} release (Fig. 4B,C). Together these findings suggest

that mZnRs are functionally expressed in the DCN neurons and participate in Zn^{2+}-triggered increases in intracellular Ca^{2+} responses.

Given the dependence of the Zn^{2+}-induced reduction of Pr on postsynaptic Ca^{2+} increases and GPCR activation (Fig. 3A), as well as the mZnR-mediated increase in Ca^{2+} responses in DCN neurons (Fig. 4A), we tested whether mZnRs are necessary for the Zn^{2+}-induced reduction of synaptic strength. We found that Zn^{2+}-mediated modulation of EPSC amplitude, PPR, and $1/CV^2$ were absent in mZnR KO mice (Fig. 5A–C). In contrast, littermate WT mice displayed reversible Zn^{2+}-induced reductions on EPSC amplitude and Pr (Fig. 5A–C). PPR levels were not different between WT mZnR and mZnR KO mice, suggesting that the absence of mZnR does not affect baseline Pr (Fig. 5B, $p = 0.22$). Importantly, mEPSC analysis revealed that basal quantal properties—mini EPSC frequency and amplitude—were not different between mZnR WT and KO mice (Fig. 6A,B). Moreover, mEPSC rise and decay times were not different between WT and KO mice (Fig. 6 C,D). These results indicate that the lack of effect of Zn^{2+} on reducing synaptic strength and Pr in mZnR KO mice is not due to differences in basal synaptic properties between WT and KO mice. The lack of Zn^{2+}-mediated changes in Pr in mZnR KO mice was not caused by nonfunctional endocannabinoid signaling in mZnR KO mice. This was determined by the fact that depolarization-induced suppression of excitation (DSE is induced by postsynaptic depolarization leading to rises in postsynaptic Ca^{2+} levels that, in turn, trigger endocannabinoid synthesis and Pr reduction) was not different between mZnR WT and KO mice (Fig. 6E). DSE in mZnR KOs was blocked by AM-251, confirming that it is mediated by CB1Rs ($n = 5$, data not shown). These results reveal that baseline Pr and depolarization-induced endocannabinoid signaling are intact in mZnR KO mice. Finally, application of 2 μM WIN (a CB1R agonist) caused a quantitatively and kinetically similar decrease in EPSC amplitude in WT and KO mice (Fig. 6F), suggesting that CB1R function is not altered between mZnR WT and mZnR KO mice. Because Zn^{2+}-induced modulation of Pr and the Zn^{2+}-induced promotion of endocannabinoid signaling are absent in mZnR KO mice, we conclude that mZnRs are necessary for the Zn^{2+}-induced reduction of Pr; this Pr reduction is likely occurring via the activation of postsynaptic endocannabinoid synthesis.

To determine the specific endocannabinoid that leads to mZnR-mediated endocannabinoid signaling and subsequent Pr reduction, we used a combined electrophysiological and biochemical approach. 2-AG, the endocannabinoid that mediates retrograde signaling in the DCN, is synthesized following PLC activation and the cleavage of diacylglycerol by a diacylglycerol lipase (DGL) (Zhao et al., 2009). To determine whether Zn^{2+}-induced changes in Pr are mediated through the 2-AG biosynthetic pathway, we first investigated the effect of pharmacological blockade of PLC and DGL on Zn^{2+}-mediated Pr modulation. We observed that incubation of slices with either a PLC inhibitor
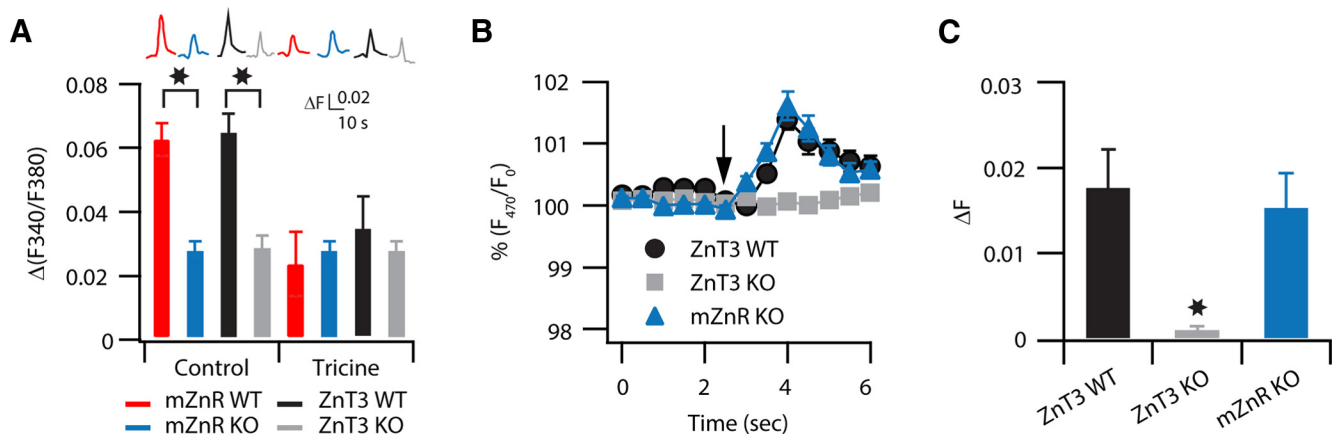
Figure 4. mZnR, a Zn^{2+}-sensing G_q-protein-coupled receptor, mediates Zn^{2+}-induced increase in intracellular Ca^{2+} in DCN neurons. **A**, Intracellular Ca^{2+} rise was monitored following a 100 Hz, 1 s stimulation of the molecular layer of the DCN in the presence or absence of tricine (10 mM, top traces). Slices from WT and KO mice were loaded with fura-2. The conditions for the different traces are indicated at the bottom of the bar graph. Bar graph showing averaged changes of Ca^{2+} rises. The residual Ca^{2+} response in the slices from mZnR KO and ZnT3 KO mice is not further attenuated by tricine and is similar to the response observed in the presence of tricine in slices from WT mice ($\Delta F/F$: mZnR WT Control: 0.062 ± 0.005, $n = 8$; mZnR KO Control: 0.027 ± 0.003, $n = 9$, $p < 0.01$; mZnR WT in tricine: 0.023 ± 0.01, $n = 9$, $p < 0.01$ when compared with mZnR WT control; mZnR KO in tricine: 0.027 ± 0.003, $n = 7$, $p = 0.48$ when compared with mZnR WT in tricine; ZnT3 WT control: 0.064 ± 0.006, $n = 4$; ZnT3 KO control: 0.028 ± 0.004, $n = 8$, $p < 0.01$ when compared with ZnT3 WT control; ZnT3 WT in tricine: 0.034 ± 0.01, $n = 8$, $p < 0.01$ when compared with WT control; ZnT3 KO in tricine: 0.026 ± 0.004, $n = 8$, $p = 0.52$ when compared with ZnT3 KO control). **B**, Representative response illustrating extracellular Zn^{2+}-dependent changes in 2 μM Newport Green (a nonpermeable, extracellular Zn^{2+} sensor) fluorescence in the DCN molecular layer after 1 s, 100 Hz stimulation of the parallel fibers in a slice from WT, ZnT3 KO, and mZnR KO mice. **C**, Average responses showing that Newport Green fluorescence in response to 1 s, 100 Hz stimulation of the parallel fibers was abolished in ZnT3 KO mice, but was normal in mZnR KO mice (ΔF: ZnT3 WT: 0.018 ± 0.004, $n = 7$ slices; ZnT3 KO: 0.001 ± 0.0004, $n = 11$ slices, $p < 0.01$ compared with ZnT3 WT; mZnR KO: 0.015 ± 0.004, $n = 8$ slices). Summary data represent mean $\pm$ SEM. Asterisks indicate statistically significant differences, $p < 0.05$.
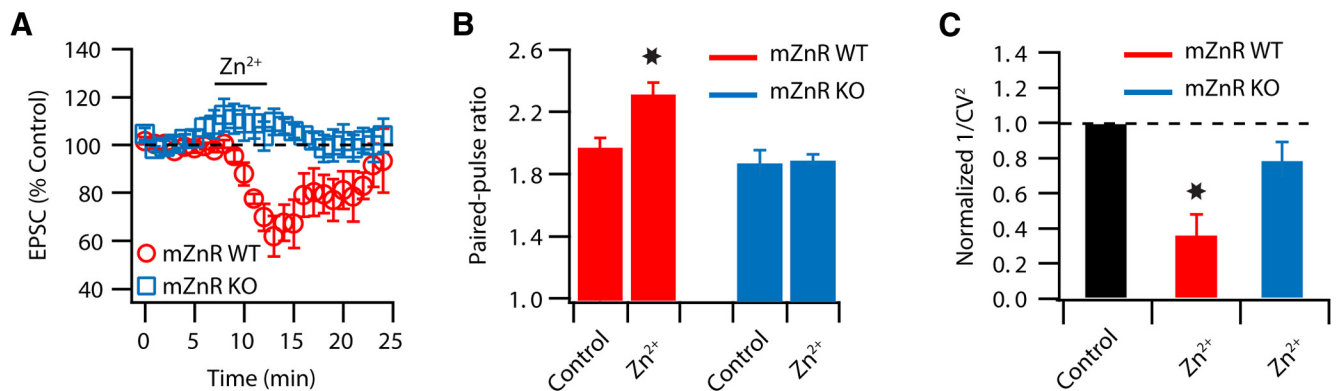

Figure 5. mZnR is necessary for Zn^{2+}-induced decrease in Pr. **A**, Zn^{2+}-induced reversible depression of EPSCs was observed in WT mice but not in mZnR KO littermates (EPSC amplitude mZnR WT: $65.7 \pm 8\%$ of baseline, $n = 6$, $p < 0.01$; mZnR KO: $107.4 \pm 5.6\%$ of baseline, $n = 5$, $p = 0.27$). **B**, PPR (20 ms interstimulus interval) is increased after Zn^{2+} application in mZnR WT mice but is unaffected in mZnR KO littermates (mZnR WT PPR baseline: 1.97 ± 0.05; PPR after Zn^{2+}: 2.32 ± 0.06; $n = 6$, $p < 0.01$; mZnR KO: PPR baseline: 1.88 ± 0.07; PPR after Zn^{2+}: 1.90 ± 0.03; $n = 5$, $p = 0.75$). **C**, $1/CV^2$ is decreased after Zn^{2+} application in mZnR WT mice but is unaffected in mZnR KO littermates (mZnR WT $1/CV^2$: $0.36 \pm 0.11\%$ of baseline, $n = 6$, $p < 0.01$; mZnR KO: $1/CV^2$: $0.79 \pm 0.11\%$ of baseline, $n = 5$, $p = 0.15$). Summary data represent mean $\pm$ SEM. Asterisks indicate statistically significant differences, $p < 0.05$.

(5 μM U73122), or a DGL inhibitor (10 μM THL) blocked Zn^{2+}-induced depression of EPSC amplitude and the concomitant Zn^{2+}-induced changes in PPR and $1/CV^2$ (Fig. 7A–C). Moreover, bath application of both these inhibitors did not affect baseline synaptic transmission, or CV of evoked EPSCs, indicating that their inhibitory effect on Zn^{2+}-induced Pr reduction is not due to a nonspecific change of baseline Pr that occludes or blocks further changes in Pr by Zn^{2+} (Fig. 7D–F). Together, these results suggest that application of Zn^{2+} leads to a PLC-dependent production of 2-AG.

Next, we used isotopic dilution LC/MS/MS to quantify 2-AG levels and their dependence on Zn^{2+}. The two different isomers of AG (2-AG and 1-AG) were chromatographically resolved and base peak separations were achieved (Fig. 8A). Consistent with previous reports (Zhang et al., 2010), the isotopically labeled 2-AG-d8 had a 0.12 min shorter retention time (Fig. 8A). The

formation of endogenous 2-AG was confirmed by co-elution with internal standard (Fig. 8A) and by high-resolution MS and MS/MS data obtained on the 2-AG peak, where a similar fragmentation pattern was observed between the standard and the DCN tissue samples (Fig. 8B,C). In agreement with our hypothesis on the enhancing effect of Zn^{2+} on the 2-AG metabolic pathway (Fig. 7), HPLC-MS analysis showed that DCN 2-AG levels increased significantly after Zn^{2+} (100 μM for 5 min) application (Fig. 8D). Moreover, Zn^{2+}-mediated increases in 2-AG levels were abolished when slices were either pretreated with the PLC inhibitor (U73122, 5 μM for 30 min before Zn^{2+} application) or in mZnR KO mice (Fig. 8D). These results indicate that exogenous Zn^{2+} leads to increased 2-AG synthesis via a PLC-dependent pathway. Given that 2-AG synthesizing enzymes have been localized in the dendrites of DCN fusiform cells (Zhao et al., 2009), our results suggest that activation of mZnR leads to the
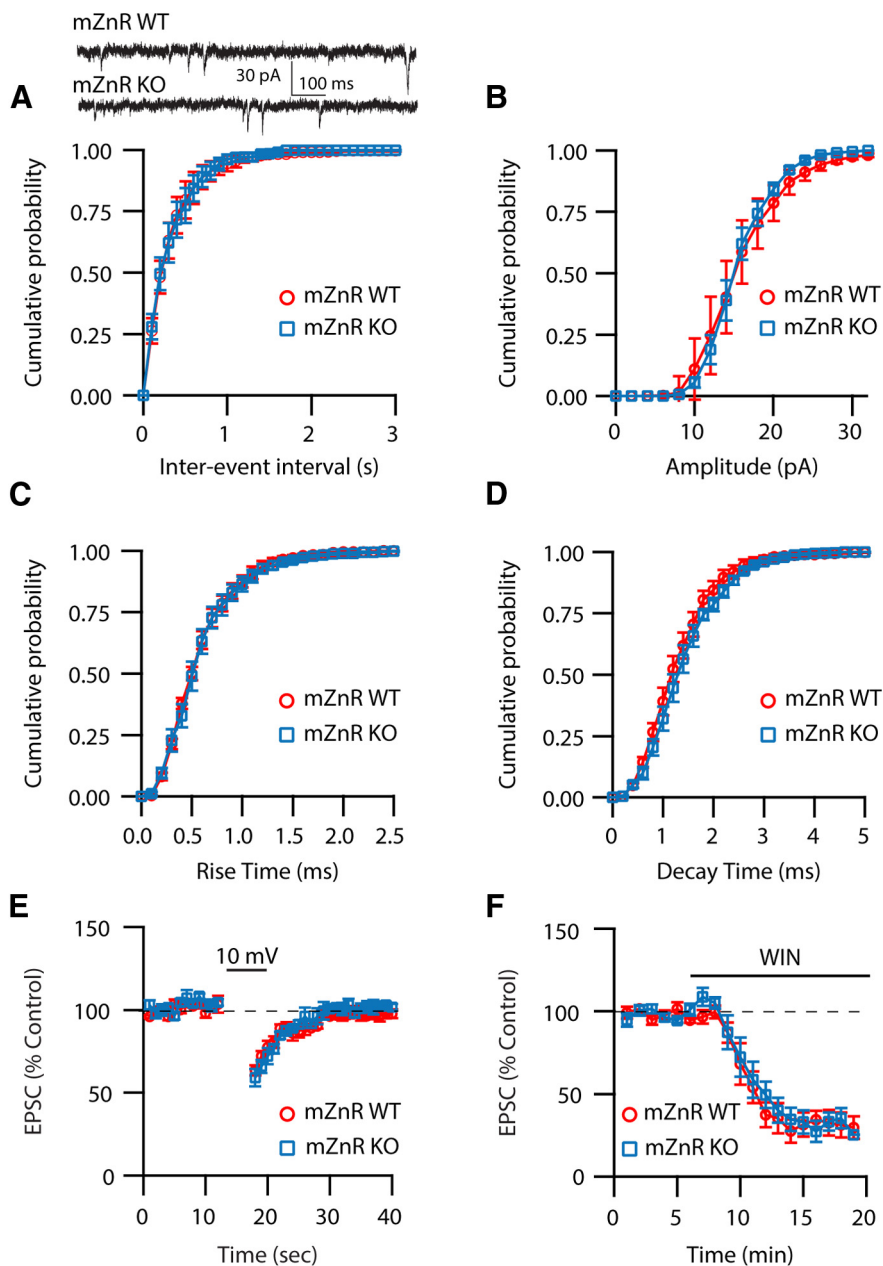
Figure 6. Quantal properties and depolarization-induced endocannabinoid signaling are not altered in mZnR KO mice. **A**, Cumulative probability plot of mEPSC frequencies shows that frequencies are not different between mZnR WT and KO mice (mean mEPSC frequency mZnR WT: 3.03 ± 0.45 Hz, n = 5; mZnR KO: 3.52 ± 0.59 Hz; n = 5, p = 0.51). Top, Sample traces of mEPSCs from mZnR WT and KO mice. **B**, Cumulative probability plot of mEPSC amplitudes shows that amplitudes are not different between mZnR WT and KO mice (mean mEPSC amplitude mZnR WT: 16.62 ± 2.09 pA, n = 5; mZnR KO: 15.56 ± 0.65 pA; n = 5, p = 0.64). **C**, Cumulative probability plot of mEPSC rise times shows that rise times are not different between mZnR WT and KO mice (mean mEPSC rise time mZnR WT: 0.63 ± 0.05 ms, n = 5; mZnR KO: 0.66 ± 0.05 ms; n = 5, p = 0.61). **D**, Cumulative probability plot of mEPSC decay times shows that decay times are not different between mZnR WT and KO mice (mean mEPSC decay time: mZnR WT: 1.3 ± 0.09 ms, n = 5; mZnR KO: 1.43 ± 0.07 ms; n = 5, p = 0.28). **E**, Time course of DSE, induced by 5 s depolarization to 10 mV in mZnR WT and KO mice (mZnR WT DSE: 37 ± 3.1% of control, n = 5; mZnR KO DSE: 41 ± 5.3% of control, n = 6, p = 0.35). **F**, Time course of 2 μM WIN on baseline synaptic transmission of mZnR WT and KO mice (mZnR WT: 31.8 ± 0.77% of baseline, n = 5, mZnR KO: 30.84 ± 1.9%, n = 5, p = 0.32). Summary data represent mean ± SEM.

activation of postsynaptic PLC and DGL leading to enhanced postsynaptic 2-AG production.

Endogenous synaptic Zn^{2+} levels decrease Pr via mZnR and endocannabinoid signaling

Next, we investigated whether endogenous, synaptically released Zn^{2+} reduces Pr via promotion of endocannabinoid signaling.

Brief bursts of presynaptic activity can promote the synthesis and release of endocannabinoids from postsynaptic cells, leading to presynaptic CB1 receptor activation that, in turn, suppress neurotransmitter release (Brown et al., 2003). This process leads to endocannabinoid-mediated short-term plasticity: short-term depression in this case. Therefore, to determine whether endogenous Zn^{2+} triggers endocannabinoid signaling, we investigated the role of synaptically released Zn^{2+} in short-term plasticity. We measured parallel fiber-evoked EPSCs at low frequencies (0.3 Hz) before and after a high-frequency stimulus train (100 Hz, 1 s). This stimulus train produced short-term facilitation in EPSC amplitude (STF; Fig. 9A1). Bath application of the extracellular Zn^{2+} chelator tricine after the initial stimulus train, in the same cell, significantly increased the magnitude of STF induced by an identical stimulus train (Fig. 9A1,A3). These results suggest that chelation of synaptically released Zn^{2+} during the high-frequency train enhanced the magnitude of induced STF. Brief trains of presynaptic activity, apart from promoting synthesis and release of endocannabinoids, trigger a build-up of calcium in presynaptic boutons resulting in forms of short-term plasticity (Zucker and Regehr, 2002), such as augmentation and post-tetanic potentiation (PTP). In many synapses, the combined effect of PTP and endocannabinoid signaling determines the size and the sign of short-term plasticity (Beierlein et al., 2007). Therefore, one possible interpretation of the effect of tricine in enhancing the amount of STF is that the chelation of Zn^{2+} blocks Zn^{2+}-mediated endocannabinoid signaling and short-term depression, thereby leading to enhanced STF. This hypothesis predicts that blockade of endocannabinoid signaling should increase the amount of STF and occlude the enhancing effect of tricine. Consistent with this hypothesis, application of AM-251 increased STF and occluded the enhancement of STF produced by Zn^{2+} chelation (Fig. 9A2,A3). These results suggest that endogenous, synaptically released Zn^{2+} modulates STF by enhancing endocannabinoid signaling.

If chelation of synaptic Zn^{2+} enhances STF (Fig. 9A) by affecting the balance between opposing forms of modulation of Pr, we expect that synaptic Zn^{2+} would modulate the threshold for inducing STF. To test this hypothesis, we determined the effect of Zn^{2+} chelation on threshold conditions under which presynaptic trains of action potentials fail to induce short-term plasticity. We varied the frequency of presynaptic bursts and investigated the effect of tricine on the resulting short-term plasticity. We found that although a
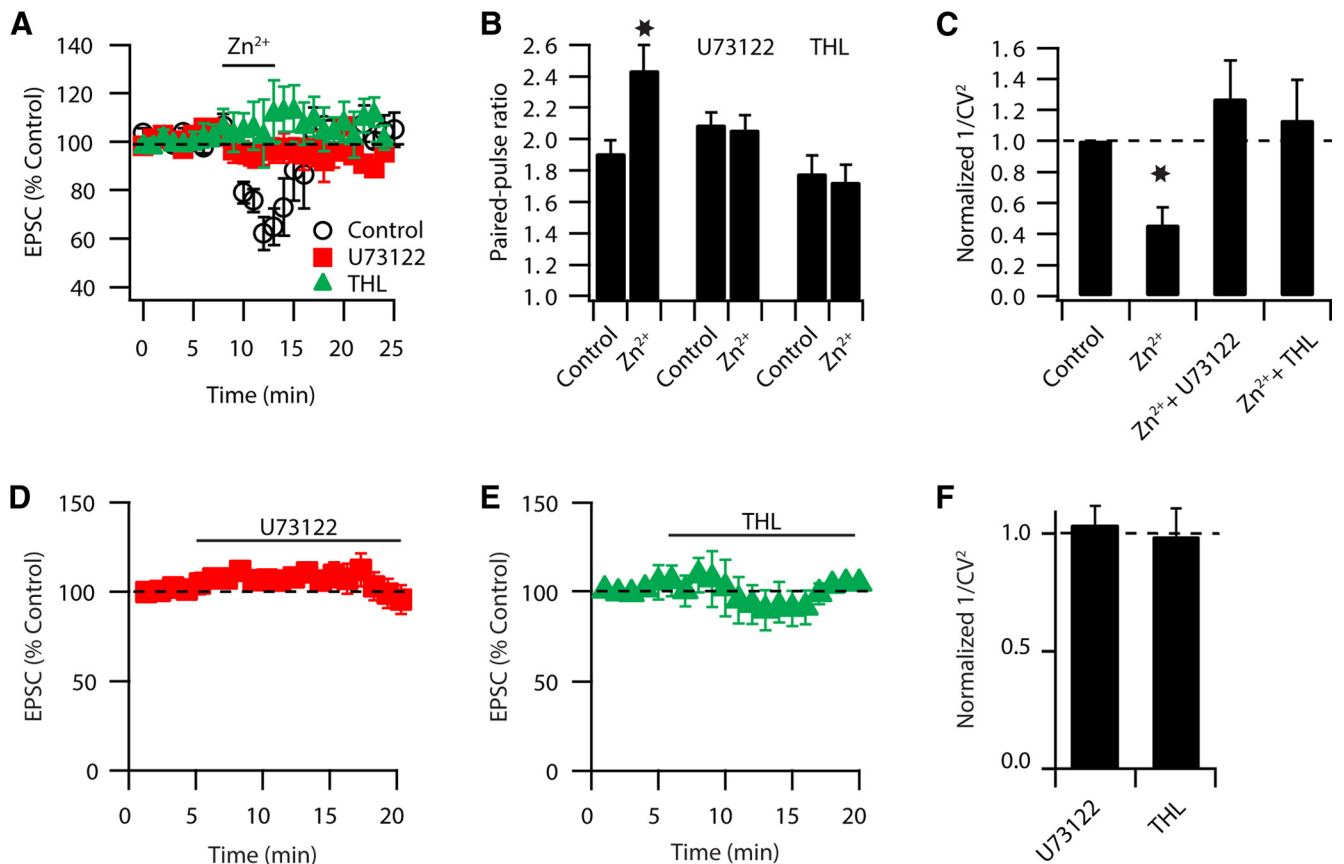
Figure 7. Zn^{2+}-induced decrease in Pr is mediated by a PLC- and DGL-dependent metabolic pathway. ***A***, Zn^{2+}-induced reversible depression of EPSCs was blocked by bath application of 5 μM U73122 or 10 μM THL (EPSC amplitude control: 67.60 ± 6.10% of baseline, $n = 5$, $p < 0.01$; U73122: 98.30 ± 3.66% of baseline, $n = 6$, $p = 0.33$; THL: 105.40 ± 7.70% of baseline, $n = 6$, $p = 0.42$). ***B***, PPR (20 ms interstimulus interval) is increased after Zn^{2+} application in control conditions, but this increase is blocked in the presence of either U73122 or THL (PPR Control baseline: 1.91 ± 0.08; after Zn^{2+}: 2.44 ± 0.16; $n = 5$; $p < 0.01$; U73122 baseline: 2.09 ± 0.08; after Zn^{2+}: 2.06 ± 0.09; $n = 6$; $p = 0.59$; THL baseline: 1.78 ± 0.11; after Zn^{2+}: 1.72 ± 0.10; $n = 6$; $p = 0.3$). ***C***, $1/CV^2$ is decreased after Zn^{2+} application in control but this decrease is blocked in the presence of either U73122 or THL ($1/CV^2$: after Zn^{2+} 0.46 ± 0.11% of baseline, $n = 6$, $p < 0.01$; + U73122 1.27 ± 0.24% of baseline, $n = 6$, $p = 0.41$; + THL: 1.13 ± 0.26% of baseline, $n = 6$, $p = 0.56$). ***D***, Bath application of U73122 does not affect baseline synaptic transmission (EPSC amplitude: 104.9 ± 2.9%, of baseline, $n = 5$, $p = 0.25$). ***E***, Bath application of THL does not affect baseline synaptic transmission (EPSC amplitude: 101.5 ± 2.1%, $n = 5$, $p = 0.35$). ***F***, Bath application of either U73122 or THL does not affect $1/CV^2$ ($1/CV^2$ U73122: 1.03 ± 0.08% of baseline, $n = 5$, $p = 0.52$; THL: 0.99 ± 0.12% of baseline, $n = 5$, $p = 0.59$). Summary data represent mean ± SEM. Asterisks indicate statistically significant differences, $p < 0.05$.

30 Hz, 1 s stimulation did not affect synaptic strength, application of tricine, under identical conditions, resulted in significant STF (Fig. 9*B1, B3*). Moreover, application of AM-251 alone under these conditions also revealed STF and, importantly, occluded the enhancing effect of tricine (Fig. 9*B2, B3*). Together, these results suggest that the release of endogenous Zn^{2+} during bursts of presynaptic activity promotes endocannabinoid signaling and shifts the balance of opposing short-term plasticity mechanisms toward reduction, or decreased enhancement, of synaptic strength.

Because PTP depends on baseline Pr (Zucker and Regehr, 2002), potential effects of tricine on baseline Pr would affect the amount of observed STF. However, tricine did not affect baseline EPSC strength, PPR, or CV, suggesting that its effects on short-term plasticity are not due to changes of baseline Pr (Fig. 10*A–C*). Moreover, these observations indicate that any release of synaptic Zn^{2+} during baseline synaptic transmission is not capable of promoting endocannabinoid signaling; presynaptic trains of action potentials are needed for Zn^{2+}-induced promotion of endocannabinoid signaling. Together, these findings (Figs. 9,10) reveal a previously unknown role for synaptic Zn^{2+} in setting the threshold for short-term plasticity via enhancement of endocannabinoid signaling.

Given that exogenous Zn^{2+} triggers endocannabinoid synthesis that is dependent on mZnRs (Figs. 2–8), we hypothesized that endogenous Zn^{2+}-mediated reduction of STF (Fig. 9) is also dependent on mZnRs. If mZnRs are necessary for the Zn^{2+}-induced endocannabinoid synthesis, then we expect that STF should be increased in mZnR KO mice; the enhancing effect of tricine on STF should also be absent in mZnR KO mice. In agreement with our hypotheses, STF in response to 100 Hz stimulation was enhanced in mZnR KO mice (Fig. 11*A1,A3*). Moreover, chelation of synaptically released Zn^{2+} by tricine did not increase the magnitude of STF in mZnR KO mice, suggesting that the lack of the zinc receptor, similar to the application of AM-251 in control mice in Figure 9, occludes the effect of tricine (Fig. 11*A2, A3*). Since depolarization-induced endocannabinoid signaling is intact in mZnR KO and baseline Pr is not affected by the absence of mZnR (Fig. 6), these results suggest that the enhancing effect of synaptic Zn^{2+} on short-term plasticity is dependent on mZnR activation of endocannabinoid signaling.

To determine the effect of elimination of synaptic Zn^{2+} release on endocannabinoid signaling and short-term plasticity, we also used ZnT3 KO mice, which do not display any DCN vesicular Zn^{2+} release (Fig. 4*B,C*). Given that Zn^{2+}-chelation experiments with tricine suggest that the release of vesicular
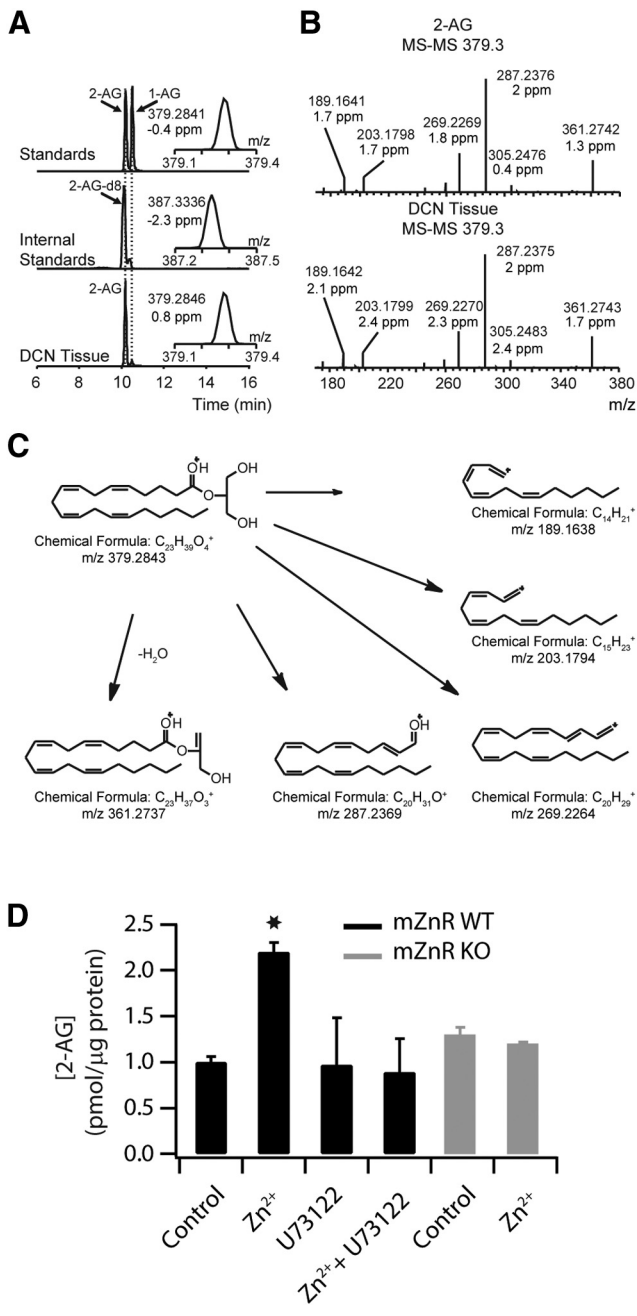
Figure 8. LC/MS/MS analysis reveals that Zn^{2+} induces a mZnR-dependent increase of 2-AG synthesis in the DCN. **A**, The two different AG isomers (2-AG and 1-AG) were chromatographically resolved and base peak separations were achieved. 2-AG and 2-AG-d8 were detected following the 379.3 to 287.2 m/z and 387.3 to 295.2 transitions, respectively, using a triple quadrupole. In parallel accurate mass determination using a Velos Orbitrap resulted in mass confirmations at the 2 ppm level for standards and for tissue-obtained 2-AG (inserts). **B**, 2-AG identity was confirmed by co-elution with internal standard (**A**) and by high-resolution MS and MS/MS data obtained on the 2-AG peak, where a similar fragmentation pattern was observed between the 2-AG standard and the DCN tissue samples. **C**, Molecular structures of product ions obtained upon ion trap collision-induced dissociations of 2-AG shown in **B**. **D**, Zn^{2+} application (100 μM for 5 min) increased 2-AG levels in a PLC and mZnR-dependent manner. HPLC-MS measurements of 2-AG levels in DCN slices from WT and mZnR KO littermates in the presence of Zn^{2+} and/or U73122 (5 μM, PLC inhibitor applied for 30 min before Zn^{2+} application; mZnR WT Control: 1 ± 0.06 pmol/μg protein, $n = 8$; mZnR WT in Zn^{2+}: 2.2 ± 0.1 pmol/μg protein, $n = 8$, $p < 0.01$; mZnR WT in U73122: 0.97 ± 0.51 pmol/μg protein, $n = 6$ when compared with mZnR WT control; $p = 0.6$; mZnR WT in U73122 and Zn^{2+}: 0.89 ± 0.37 pmol/μg protein, $n = 7$; $p = 0.42$ when compared with mZnR WT control; mZnR KO: 1.3 ± 0.08 pmol/μg protein in control, $n = 6$; mZnR KO in Zn^{2+}: 1.2 ± 0.02 pmol/μg protein, $n = 4$, $p = 0.5$ when compared with mZnR KO control). Summary data represent mean $\pm$ SEM. Asterisks indicate statistically significant differences, $p < 0.05$.

Zn^{2+} decreases STF levels (Fig. 9), ZnT3 KO mice are expected to show more robust STF than WT littermate mice. Moreover, we expected that the enhancing effect of tricine on STF would be occluded in ZnT3 KO mice. Indeed, comparison of STF levels between ZnT3 WT and ZnT3 KO littermates revealed increased levels of STF (100 Hz stimulation) in ZnT3 KO mice (Fig. 11*B1*, *B3*). Additionally, the enhancing effect of tricine was occluded in ZnT3 KO mice (Fig. 11 *B2,B3*). Together these results suggest that endogenous, synaptically released Zn^{2+} mediates the depressing effects in short-term plasticity observed in fusiform cells.

During milder presynaptic stimulation (30 Hz, 1 s) synaptic Zn^{2+} increased the threshold for STF (Fig. 9*B1–B3*). Based on this finding, we hypothesized that the threshold for inducing STF would be lower in mZnR KO and in ZnT3 KO mice. To test this hypothesis we investigated the amount of STF after a 30 Hz 1 s presynaptic stimulus. In accordance with our hypothesis, while slices from mZnR WT and ZnT3 WT mice showed minimal levels of STF, mZnR KO and ZnT3 KO mice showed significantly enhanced levels of STF (Fig. 11*C1–C5*). The observed effects in ZnT3KO mice are not due to changes in basal quantal properties, baseline Pr, or in deficient endocannabinoid signaling in ZnT3 KO mice, as WT and KO mice displayed similar mEPSC frequency, amplitude, rise time, decay time, similar levels of baseline PPR, and DSE (Fig. 12*A–F*). Together, our physiological, pharmacological, genetic, and biochemical results show that release of endogenous, vesicular Zn^{2+} reduces neurotransmitter release via mZnR-dependent, G_q-coupled receptor activation of 2-AG synthesis. While a G_q-coupled receptor promotion of endocannabinoid synthesis has been well established during the last decade, our results reveal a surprising link between synaptically released Zn^{2+} and retrograde endocannabinoid signaling, thus providing a significant advance toward the elucidation of the role of Zn^{2+} in synaptic physiology.

Discussion

We report that synaptic Zn^{2+} modulates probability of release of glutamatergic terminals via activation of retrograde endocannabinoid signaling. We propose that Zn^{2+}-mediated modulation of Pr via endocannabinoid signaling reveals a previously unrecognized synaptic signaling pathway that includes presynaptic ZnT3 and CB1Rs as well as postsynaptic mZnRs, PLC and DGL. This signaling pathway provides a fundamental substrate for both neuromodulatory and state-dependent regulation of neuronal properties, thus shaping synaptic strength in an activity-dependent manner.

The role of Zn^{2+} and mZnR in modulating synaptic transmission

Our studies provide the first evidence for inhibitory effects of Zn^{2+}-mediated signaling on Pr. We demonstrate a synaptic Zn^{2+}-mediated negative feedback loop that reduces Pr at DCN parallel fiber synapses through a signaling pathway linking Zn^{2+} release to endocannabinoid synthesis. Bath application of exogenous Zn^{2+} as well as release of endogenous Zn^{2+} caused a reversible reduction of Pr. This inhibitory effect of Zn^{2+} is opposite to the effect that has been observed in mossy fiber synapses (Li et al., 2001; Huang et al., 2008), where exogenous Zn^{2+} application leads to LTP of synaptic response via presynaptic increases in Pr (Huang et al., 2008; Pan et al., 2011). Given that mZnRs are likely present in mossy fiber synapses (Besser et al., 2009; Chorin et al., 2011), the lack of the inhibitory effect of Zn^{2+} on Pr is likely due to the absence of endocannabinoid signaling in mossy fiber synapses (Hofmann et al., 2008). Our results suggest
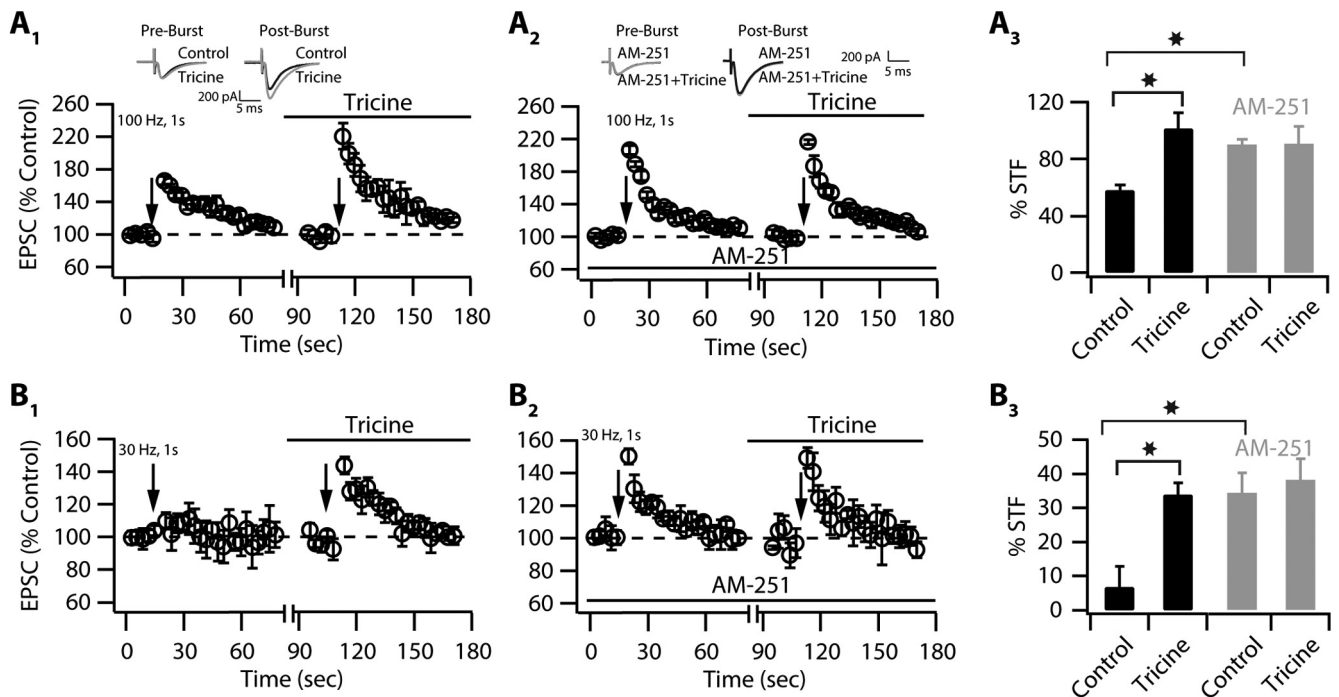
Figure 9. Synaptically released Zn^{2+} modulates STF via endocannabinoid signaling. ***A1***, STF is enhanced after Zn^{2+} chelation (STF control: $58.24 \pm 3.4\%$, $n = 9$; tricine: $101.5 \pm 11.16\%$, $n = 9$, $p < 0.01$). Summary graph showing the time course of the change in EPSC amplitude after 100 Hz, 1 s parallel fiber stimulation, in control and after endogenous Zn^{2+} chelation with tricine (100 Hz, 1 s stimulation was applied before and after tricine for the same and for each cell; 10 mм tricine was bath applied for at least 10 min before 100 Hz, 1 s stimulation). The high-frequency stimulus was delivered under current clamp to allow postsynaptic spiking. Top, Representative traces of EPSCs before the train (pre-burst), and after the 100 Hz train (post-burst). ***A2***, AM-251-enhanced baseline STF and blocked the enhancement of STF after Zn^{2+} chelation (STF control in AM-251: $90.32 \pm 3.40\%$, $n = 10$, $p < 0.05$ when compared with control from ***A1***; tricine in AM-251: $90.55 \pm 11.16\%$, $n = 10$, $p = 0.28$ when compared with control in AM-251). Summary graph showing the time of the change in the EPSC amplitude after 100 Hz, 1 s parallel fiber stimulation as in ***A1***, but now in the presence of AM-251 (pre-incubation of slices with 1 μм AM-251 for at 1 h and bath application during the experiment). Top, Representative traces of EPSCs before the train (pre-burst), and after the 100 Hz train (post-burst). ***A3***, Average values of STF from ***A1*** and ***A2***. Percentage STF magnitude is the average of first three points after the train. ***B1***, STF is revealed after Zn^{2+} chelation; synaptic Zn^{2+} modulates the threshold for STF (STF control: $6.66 \pm 6.10\%$, $n = 6$, $p = 0.25$; tricine: $33.95 \pm 3.31\%$, $n = 6$, $p < 0.01$). Summary graph showing the time course of the change in the EPSC amplitude after 30 Hz, 1 s parallel fiber stimulation, in control and after endogenous Zn^{2+} chelation with tricine (30 Hz, 1 s stimulation was applied before and after tricine for the same and for each cell; 10 mм tricine was bath applied for at least 10 min before 30 Hz, 1 s stimulation). The high-frequency stimulus was delivered under current clamp to allow postsynaptic spiking. ***B2***, AM-251 enhanced baseline STF and blocked the enhancement of STF after Zn^{2+} chelation. Summary graph showing the time of the change in the EPSC amplitude after 100 Hz, 1 s parallel fiber stimulation as in ***B1***, but now in the presence of AM-251 (pre-incubation of slices with 1 μм AM-251 for at 1 h and bath application during the experiment; STF control in AM-251: $34.27 \pm 5.97\%$, $n = 6$, $p < 0.01$ when compared with control from ***B1***; tricine in AM-251: $38.16 \pm 6.23\%$, $n = 6$, $p = 0.38$ when compared with control in AM-251). ***B3***, Average values of STF from ***B1*** and ***B2***. Percentage STF magnitude is the average of first three points after the train. Summary data represent mean $\pm$ SEM. Asterisks indicate statistically significant differences, $p < 0.05$.

that the synaptic effects of Zn^{2+} are synapse specific and, similar to other neuromodulatory systems, Zn^{2+}-mediated effects depend on the molecular composition of specific synapses.

While previous studies have shown that Zn^{2+} is released in an activity and Ca^{2+}-dependent manner (Qian and Noebels, 2005, 2006), there has been a controversy about whether synaptic Zn^{2+} is released or whether Zn^{2+} creates a layer in the extracellular space that maps onto the synaptic Zn^{2+} stained region (Zn^{2+} veneer theory) (Kay, 2003; Kay and Tóth, 2008). Indeed, the amount of synaptic Zn^{2+} that reaches the postsynaptic membrane during synaptic stimulation remains unknown with estimates from ~0 or no Zn^{2+} release (Kay, 2003; Kay and Tóth, 2008), to >100 μм (Vogt et al., 2000). Here, we focused on determining whether synaptically released (endogenous) Zn^{2+}, regardless of the actual concentration reached in synaptic cleft,
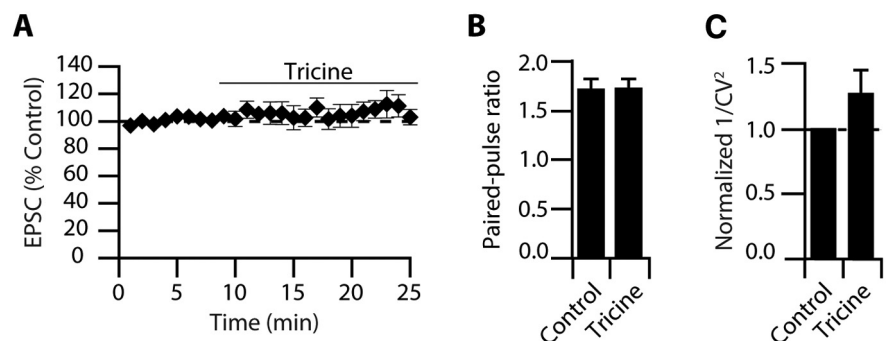

Figure 10. Tricine does not affect either baseline synaptic transmission or Pr. ***A***, Time course of the effect of tricine (10 mм) on EPSC amplitude (EPSC amplitude: $106.4 \pm 6.7\%$ of control, $n = 6$, $p = 0.57$). ***B***, ***C***, PPR (PPR control: 1.71 ± 0.11; tricine: 1.72 ± 0.10, $n = 6$, $p = 0.51$) (***B***) and $1/CV^2$ ($1/CV^2$ in tricine: $1.28 \pm 0.18\%$ of control, $n = 6$, $p = 0.3$) (***C***) did not change after tricine application. Summary data represent mean $\pm$ SEM. Asterisks indicate statistically significant differences, $p < 0.05$.

was sufficient to trigger endocannabinoid signaling. The results presented in Figures 9 and 11 show that endogenous Zn^{2+} reduces Pr via endocannabinoid signaling in the DCN. Thus, our pharmacological and genetic manipulations support a ZnT3/
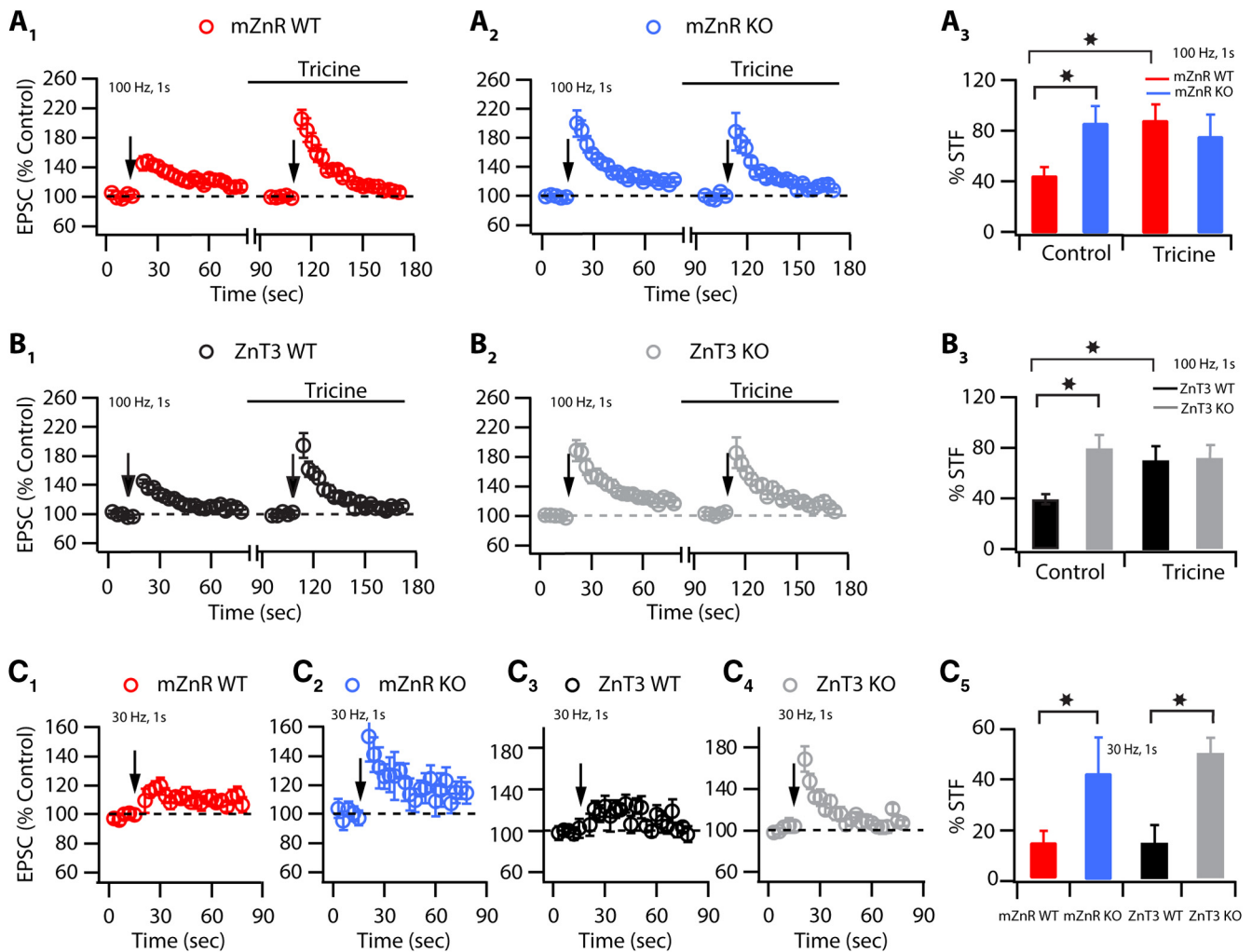
Figure 11. Synaptically released Zn^{2+}-induced modulation of STF is absent in mZnR KO and in ZnT3 KO mice. In *A1–A3* baseline STF, elicited by 100 Hz, 1 s stimulation is increased in mZnR KO mice; tricine-mediated enhancement of STF is absent in mZnR KO littermates. *A1,* Summary graph showing the time course of the change in EPSC amplitude after 100 Hz, 1 s parallel fiber stimulation, in control and after endogenous Zn^{2+} chelation with tricine in mZnR WT mice (100 Hz, 1 s stimulation was applied before and after tricine for the same and for each cell; 10 mM tricine was bath applied for at least 10 min before 100 Hz, 1 s stimulation; STF mZnR WT: 45.41 ± 6.65%, n = 10; mZnR KO: 87.28 ± 13.54%, n = 10, p < 0.01). *A2,* Summary graph showing the time course of the change in EPSC amplitude after 100 Hz, 1 s parallel fiber stimulation, in control and after endogenous Zn^{2+} chelation with tricine as in *A1,* but now in mZnR KO mice (STF: mZnR KO control: 87.28 ± 13.54%, n = 10; mZnR KO in tricine: 76.83 ± 17.10%, n = 10, p = 0.30). *A3,* Average values of STF from *A1* and *A2*. Percentage STF magnitude is the average of the first three points after the train. In *B1–B3* baseline STF elicited by 100 Hz, 1 s stimulation is increased in ZnT3 KO mice; tricine-mediated enhancement of STF is absent in ZnT3 KO littermates. *B1,* Summary graph showing the time course of the change in EPSC amplitude after 100 Hz, 1 s parallel fiber stimulation, in control and after endogenous Zn^{2+} chelation with tricine in ZnT3 WT mice (conditions are the same as in *A1*; STF ZnT3 WT: 39.28 ± 3.97%, n = 9; ZnT3 KO: 87.36 ± 10.92%, n = 9, p < 0.01). *B2,* Summary graph showing the time course of the change in EPSC amplitude after 100 Hz, 1 s parallel fiber stimulation, in control and after endogenous Zn^{2+} chelation with tricine in ZnT3 KO mice (conditions are the same as in *A1*; STF ZnT3 KO control: 87.36 ± 10.92%, n = 9; ZnT3 KO in tricine: 71.6 ± 12.29%, n = 9, p = 0.42). *B3,* Average values of STF from *B1* and *B2*. Percentage STF magnitude is the average of the first three points after the train. In *C1–C5* baseline STF elicited by 30 Hz, 1 s stimulation is revealed in mZnR KO and in ZnT3 KO mice. *C1, C2,* Summary graphs showing the time course of the change in EPSC amplitude after 30 Hz, 1 s parallel fiber stimulation, in mZnR WT and in mZnR KO littermates (STF mZnR WT: 14.35 ± 4.41%, n = 6; mZnR KO: 42.7 ± 14.10%, n = 6 p < 0.01 when compared with mZnR WT). *C3, C4,* Summary graphs showing the time course of the change in EPSC amplitude after 30 Hz, 1 s parallel fiber stimulation, in ZnT3 WT and in ZnT3 KO littermates (STF ZnT3 WT: 14.25 ± 6.91%, n = 6; ZnT3 KO: 49.34 ± 6.01%, n = 6, p < 0.01 when compared with ZnT3 WT). *C5,* Average values of STF from *C1–C4*. Percentage STF magnitude is the average of the first three points after the train. Summary data represent mean ± SEM. Asterisks indicate statistically significant differences, p < 0.05.

mZnR–dependent, endocannabinoid-mediated decrease of Pr as a result of release of endogenous Zn^{2+} in response to brief stimulus trains.

While recent results have indicated that synaptically released Zn^{2+} induced by a single action potential blocks NMDAR responses (Pan et al., 2011), our results show that mZnR-dependent triggering of endocannabinoid signaling requires trains of presynaptic action potentials. The requirement for trains of presynaptic action potentials is consistent with the recent proposal that Zn^{2+}-containing synaptic mossy fiber vesicles populate the reserve, not the readily released, pool (Lavoie et al.,

2011). Although the detailed physiological conditions leading to mZnR-mediated signaling remain undetermined, our findings suggest that, in response to a brief 30 Hz train, endogenous Zn^{2+} levels set the threshold for eliciting short-term plasticity (Figs. 9B1, 11C). While *in vivo* recordings from DCN granule cells have not been obtained, sensory stimulation can produce bursts of spikes in cerebellar granule cells at very high firing frequencies (>200 Hz) (Chadderton et al., 2004). Given the strong parallels between DCN and cerebellar granule cells (Oertel and Young, 2004), the brief 30 Hz stimulation that we used is expected to be well within the physiological range of parallel fiber activity, thus

suggesting that Zn^{2+}-mediated endocannabinoid pathway can be engaged by physiologically relevant stimuli.

Our results demonstrate that GPR39 (mZnR) is necessary for Zn^{2+}-mediated endocannabinoid synthesis; it is likely that synaptically released Zn^{2+} mediates its effects on endocannabinoid signaling and Pr via direct activation of GPR39 (mZnR; Fig. 13). GPR39, a previously orphan GPCR was initially proposed to mediate obestatin signaling and to regulate food intake (Zhang et al., 2005). However, the absence of GPR39 in the hypothalamus (Jackson et al., 2006) and the identification of Zn^{2+}, rather than obestatin, as its putative endogenous ligand (Yasuda et al., 2007) have raised questions regarding the physiological role of GPR39. Recent studies have suggested that synaptically released Zn^{2+} triggers metabotropic signaling via mZnR in the hippocampus (Besser et al., 2009), enhancing the activity of the potassium chloride cotransporter 2 in CA3 pyramidal neurons (Chorin et al., 2011). We show that during synaptic activation of excitatory terminals, similar to group 1 mGluRs (Maejima et al., 2001; Varma et al., 2001; Kushmerick et al., 2004), the mZnR is necessary for 2-AG synthesis and thus, contributes to the overall signaling profile of excitatory synaptic transmission that is tightly coupled to postsynaptic endocannabinoid synthesis. Because the 2-AG synthesizing enzymes, DGLα and DGLβ, have been localized to the dendrites of DCN fusiform cells (Zhao et al., 2009), our electrophysiological, imaging, and biochemical results are consistent with a postsynaptic localization of mZnRs.

The role of Zn^{2+} in brain function

The allosteric modulation of NMDA and glycine receptors by Zn^{2+} has suggested a role for Zn^{2+} in learning, and motor control, respectively (Hirzel et al., 2006; Adlard et al., 2010). Synaptically released Zn^{2+} has also been associated with Alzheimer's disease and pain processing (Deshpande et al., 2009; Duce et al., 2010; Nozaki et al., 2011). Although initial studies did not uncover cognitive deficits in ZnT3KO mice (Cole et al., 2001), recent evidence reveals impaired fear memory (Martel et al., 2010), impaired spatial memory and impaired behavior dependent on hippocampus and perirhinal cortex (Martel et al., 2011), accelerated aging-related decline of spatial memory (Adlard et al., 2010), as well as impairments in spatial working memory and contextual discrimination (Sindreu et al., 2011). Our studies, by demonstrating a Zn^{2+}-mediated negative feedback loop that reduces Pr at central auditory synapses—through a
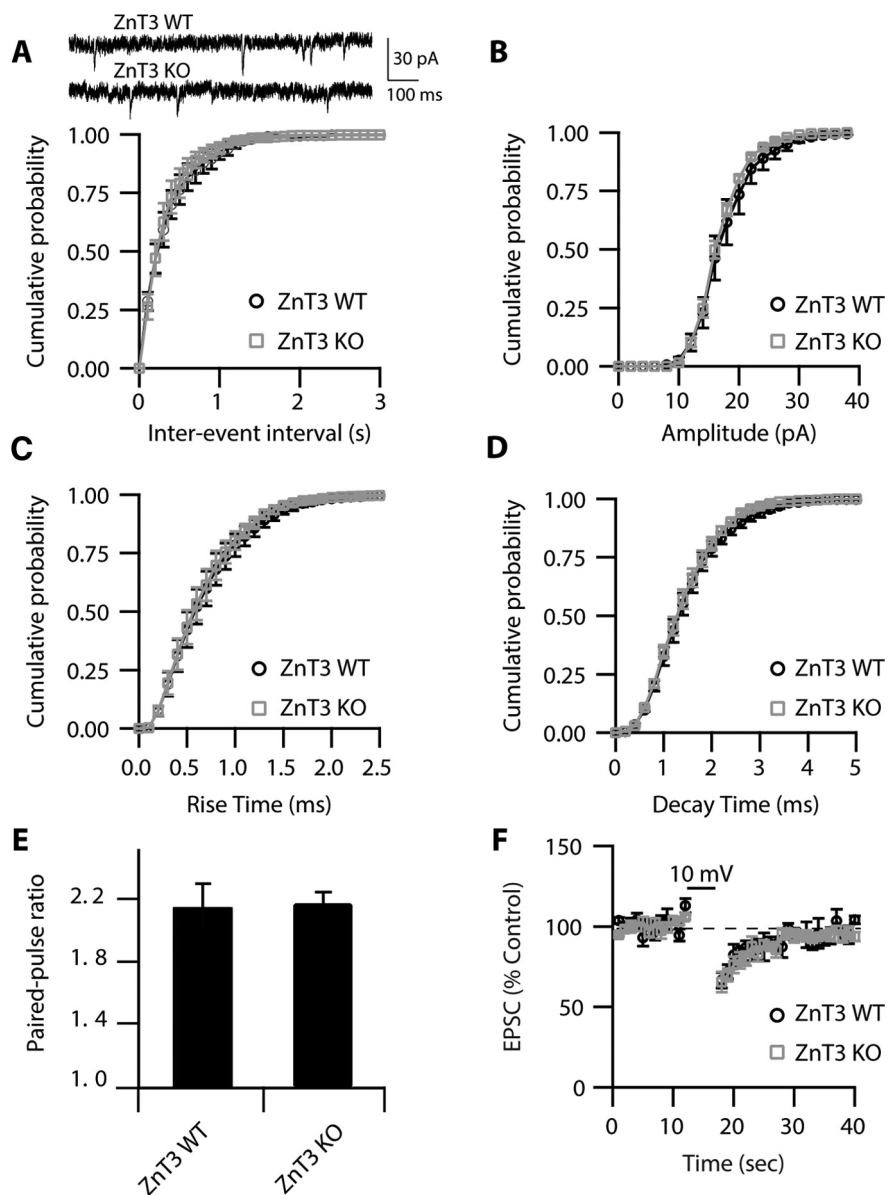

Figure 12. Quantal properties, baseline Pr and depolarization-induced endocannabinoid signaling are not altered in ZnT3 KO mice. *A*, Top, Sample traces of mEPSCs from ZnT3 WT and KO mice. Cumulative probability plot of mEPSC frequencies shows that frequencies are not different between ZnT3 WT and KO mice (mean mEPSC frequency WT: 3.25 ± 0.60 Hz, n = 5; KO: 3.57 ± 0.73 Hz; n = 5, p = 0.74). *B*, Cumulative probability plot of mEPSC amplitudes shows that amplitudes are not different between ZnT3 WT and KO mice (mean mEPSC amplitude WT: 17.50 ± 1.2 pA, n = 5; KO: 16.7 ± 0.33 pA; n = 5, p = 0.54). *C*, Cumulative probability plot of mEPSC rise times showing that rise times are not different between ZnT3 WT and KO mice (mean mEPSC rise time: WT: 0.67 ± 0.06 ms, n = 5; KO: 0.59 ± 0.03 ms; n = 5, p = 0.3). *D*, Cumulative probability plot of mEPSC decay times showing that decay times are not different between ZnT3 WT and KO mice (mean mEPSC decay time WT: 1.44 ± 0.08 ms, n = 5; KO: 1.42 ± 0.07 ms; n = 5, p = 0.84). *E*, PPR is similar in ZnT3 WT and KO littermates (PPR WT: 2.13 ± 0.15, n = 7; KO: 2.16 ± 0.11, n = 7, p = 0.85). *F*, DSE is similar in ZnT3 WT and KO mice. Time course of DSE, induced by a 5 s depolarization to 10 mV (DSE WT: 33.5 ± 4.9% of control, n = 5; KO DSE: 35 ± 3.2% of control, p = 0.54). Summary data represent mean ± SEM.

specific pathway linking mZnR activation, endocannabinoid synthesis, and Pr inhibition—pave the way for novel *in vivo* and behavioral experimental paradigms aimed at further defining the role of Zn^{2+} on brain function.

In sensory systems, the levels of synaptic Zn^{2+} in somatosensory cortex can be rapidly and dynamically regulated by sensory experience, although the physiological consequences of these changes have not been determined (Brown and Dyck, 2003; Nakashima and Dyck, 2009, 2010). Although it has been known for 25 years that DCN parallel fibers contain very large amounts of
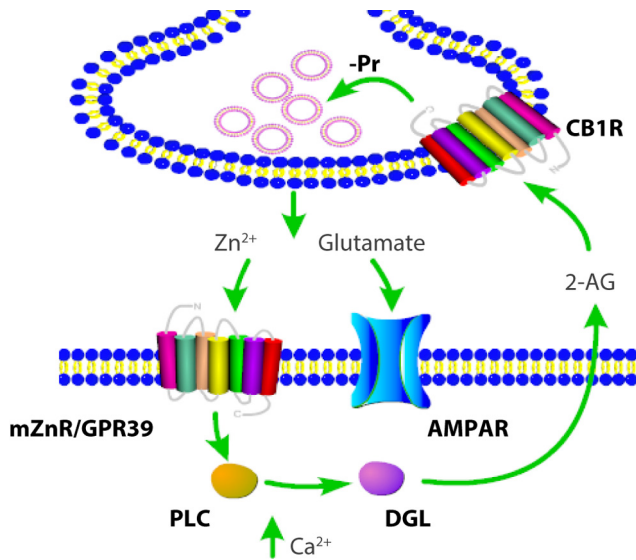
Figure 13. Schematic representation illustrating the mechanism of Zn^{2+}-induced decrease in Pr. Synaptically released Zn^{2+}, mZnR activation, rises in postsynaptic Ca^{2+} and PLC stimulation are necessary for 2-AG synthesis. 2-AG is produced by cleavage of diacylglycerol by DGL. 2-AG diffuses to the presynaptic terminal where it decreases Pr.

synaptic Zn^{2+} (Frederickson et al., 1988), the physiological role of this metal in modulating auditory circuits has not been previously evaluated. Based on our observations, we propose that synaptic Zn^{2+}, by providing a negative feedback loop that reduces synaptic strength, may decrease the responsiveness of the cochlear nucleus to acoustic stimuli: thus, synaptic Zn^{2+} release is expected to reduce the gain of input–output transformations between the auditory nerve and the cochlear nucleus. This is consistent with the proposed inhibitory role of Zn^{2+} in visual and auditory processing centers (Hirzel et al., 2006; Chappell et al., 2008), thus supporting the notion that Zn^{2+} is an inhibitory neuromodulator in sensory systems.

In conclusion, our results reveal the existence of a cellular pathway linking synaptically released Zn^{2+} and endocannabinoids: a previously unrecognized connection between two fundamental neuromodulatory systems, leading to activity-dependent inhibition of synaptic strength.

References

Adlard PA, Parncutt JM, Finkelstein DI, Bush AI (2010) Cognitive loss in zinc transporter-3 knock-out mice: a phenocopy for the synaptic and memory deficits of Alzheimer's disease? J Neurosci 30:1631–1636. CrossRef Medline

Alger BE (2012) Endocannabinoids at the synapse a decade after the dies mirabilis (29 March 2001): what we still do not know. J Physiol 590:2203–2212. Medline

Beierlein M, Fioravante D, Regehr WG (2007) Differential expression of posttetanic potentiation and retrograde signaling mediate target-dependent short-term synaptic plasticity. Neuron 54:949–959. CrossRef Medline

Bender KJ, Trussell LO (2011) Synaptic plasticity in inhibitory neurons of the auditory brainstem. Neuropharmacology 60:774–779. CrossRef Medline

Besser L, Chorin E, Sekler I, Silverman WF, Atkin S, Russell JT, Hershfinkel M (2009) Synaptically released zinc triggers metabotropic signaling via a zinc-sensing receptor in the hippocampus. J Neurosci 29:2890–2901. CrossRef Medline

Brown CE, Dyck RH (2003) Experience-dependent regulation of synaptic zinc is impaired in the cortex of aged mice. Neuroscience 119:795–801. CrossRef Medline

Brown SP, Brenowitz SD, Regehr WG (2003) Brief presynaptic bursts evoke synapse-specific retrograde inhibition mediated by endogenous cannabinoids. Nat Neurosci 6:1048–1057. CrossRef Medline

Chadderton P, Margrie TW, Häusser M (2004) Integration of quanta in cerebellar granule cells during sensory processing. Nature 428:856–860. CrossRef Medline

Chappell RL, Anastassov I, Lugo P, Ripps H (2008) Zinc-mediated feedback at the synaptic terminals of vertebrate photoreceptors. Exp Eye Res 87:394–397. CrossRef Medline

Chorin E, Vinograd O, Fleidervish I, Gilad D, Herrmann S, Sekler I, Aizenman E, Hershfinkel M (2011) Upregulation of KCC2 activity by zinc-mediated neurotransmission via the mZnR/GPR39 receptor. J Neurosci 31:12916–12926. CrossRef Medline

Cole TB, Wenzel HJ, Kafer KE, Schwartzkroin PA, Palmiter RD (1999) Elimination of zinc from synaptic vesicles in the intact mouse brain by disruption of the ZnT3 gene. Proc Natl Acad Sci U S A 96:1716–1721. CrossRef Medline

Cole TB, Martyanova A, Palmiter RD (2001) Removing zinc from synaptic vesicles does not impair spatial learning, memory, or sensorimotor functions in the mouse. Brain Res 891:253–265. CrossRef Medline

Deshpande A, Kawai H, Metherate R, Glabe CG, Busciglio J (2009) A role for synaptic zinc in activity-dependent Abeta oligomer formation and accumulation at excitatory synapses. J Neurosci 29:4004–4015. CrossRef Medline

Duce JA, Tsatsanis A, Cater MA, James SA, Robb E, Wikhe K, Leong SL, Perez K, Johanssen T, Greenough MA, Cho HH, Galatis D, Moir RD, Masters CL, McLean C, Tanzi RE, Cappai R, Barnham KJ, Ciccotosto GD, Rogers JT, et al. (2010) Iron-export ferroxidase activity of beta-amyloid precursor protein is inhibited by zinc in Alzheimer's disease. Cell 142:857–867. CrossRef Medline

Dutar P, Nicoll RA (1988) Pre- and postsynaptic GABAB receptors in the hippocampus have different pharmacological properties. Neuron 1:585–591. CrossRef Medline

Evstratova A, Tóth K (2011) Synaptically evoked Ca^{2+} release from intracellular stores is not influenced by vesicular zinc in CA3 hippocampal pyramidal neurones. J Physiol 589:5677–5689. Medline

Faber DS, Korn H (1991) Applicability of the coefficient of variation method for analyzing synaptic plasticity.[erratum appears in Biophys J 1992 Mar;61:following 831]. Biophysical J 60:1288–1294. CrossRef Medline

Frederickson CJ, Howell GA, Haigh MD, Danscher G (1988) Zinc-containing fiber systems in the cochlear nuclei of the rat and mouse. Hear Res 36:203–211. CrossRef Medline

Hirzel K, Müller U, Latal AT, Hülsmann S, Grudzinska J, Seeliger MW, Betz H, Laube B (2006) Hyperekplexia phenotype of glycine receptor alpha1 subunit mutant mice identifies Zn^{2+} as an essential endogenous modulator of glycinergic neurotransmission. Neuron 52:679–690. CrossRef Medline

Hofmann ME, Nahir B, Frazier CJ (2008) Excitatory afferents to CA3 pyramidal cells display differential sensitivity to CB1 dependent inhibition of synaptic transmission. Neuropharmacology 55:1140–1146. CrossRef Medline

Huang YZ, Pan E, Xiong ZQ, McNamara JO (2008) Zinc-mediated transactivation of TrkB potentiates the hippocampal mossy fiber-CA3 pyramid synapse. Neuron 57:546–558. CrossRef Medline

Hyrc KL, Bownik JM, Goldberg MP (2000) Ionic selectivity of low-affinity ratiometric calcium indicators: mag-Fura-2, Fura-2FF and BTC. Cell Calcium 27:75–86. CrossRef Medline

Jackson VR, Nothacker HP, Civelli O (2006) GPR39 receptor expression in the mouse brain. Neuroreport 17:813–816. CrossRef Medline

Kay AR (2003) Evidence for chelatable zinc in the extracellular space of the hippocampus, but little evidence for synaptic release of Zn. J Neurosci 23:6847–6855. Medline

Kay AR, Tóth K (2008) Is zinc a neuromodulator? Sci Signal 1:re3. CrossRef Medline

Kim J, Isokawa M, Ledent C, Alger BE (2002) Activation of muscarinic acetylcholine receptors enhances the release of endogenous cannabinoids in the hippocampus. J Neurosci 22:10182–10191. Medline

Kushmerick C, Price GD, Taschenberger H, Puente N, Renden R, Wadiche JI, Duvoisin RM, Grandes P, von Gersdorff H (2004) Retroinhibition of presynaptic Ca2+ currents by endocannabinoids released via postsynaptic mGluR activation at a calyx synapse. J Neurosci 24:5955–5965. CrossRef Medline

Lavoie N, Jeyaraju DV, Peralta MR 3rd, Seress L, Pellegrini L, Tóth K (2011) Vesicular zinc regulates the Ca^{2+} sensitivity of a subpopulation of presynaptic vesicles at hippocampal mossy fiber terminals. J Neurosci 31: 18251–18265. CrossRef Medline

Li Y, Hough CJ, Frederickson CJ, Sarvey JM (2001) Induction of mossy fiber –> Ca3 long-term potentiation requires translocation of synaptically released Zn^{2+}. J Neurosci 21:8015–8025. Medline

Maejima T, Hashimoto K, Yoshida T, Aiba A, Kano M (2001) Presynaptic inhibition caused by retrograde signal from metabotropic glutamate to cannabinoid receptors. Neuron 31:463–475. CrossRef Medline

Martel G, Hevi C, Friebely O, Baybutt T, Shumyatsky GP (2010) Zinc transporter 3 is involved in learned fear and extinction, but not in innate fear. Learn Mem 17:582–590. CrossRef Medline

Martel G, Hevi C, Kane-Goldsmith N, Shumyatsky GP (2011) Zinc transporter ZnT3 is involved in memory dependent on the hippocampus and perirhinal cortex. Behav Brain Res 223:233–238. CrossRef Medline

Maske H (1955) Topochemical detection of zinc in the Ammon's horn of different mammals. Naturwissennschaften 42.

Moechars D, Depoortere I, Moreaux B, de Smet B, Goris I, Hoskens L, Daneels G, Kass S, Ver Donck L, Peeters T, Coulie B (2006) Altered gastrointestinal and metabolic function in the GPR39-obestatin receptorknockout mouse. Gastroenterology 131:1131–1141. CrossRef Medline

Mott DD, Benveniste M, Dingledine RJ (2008) pH-dependent inhibition of kainate receptors by zinc. J Neurosci 28:1659–1671. CrossRef Medline

Nakashima AS, Dyck RH (2009) Zinc and cortical plasticity. Brain Res Rev 59:347–373. CrossRef Medline

Nakashima AS, Dyck RH (2010) Dynamic, experience-dependent modulation of synaptic zinc within the excitatory synapses of the mouse barrel cortex. Neuroscience 170:1015–1019. CrossRef Medline

Nozaki C, Vergnano AM, Filliol D, Ouagazzal AM, Le Goff A, Carvalho S, Reiss D, Gaveriaux-Ruff C, Neyton J, Paoletti P, Kieffer BL (2011) Zinc alleviates pain through high-affinity binding to the NMDA receptor NR2A subunit. Nat Neurosci 14:1017–1022. CrossRef Medline

Oertel D, Young ED (2004) What's a cerebellar circuit doing in the auditory system? Trends Neurosci 27:104–110. CrossRef Medline

Pan E, Zhang XA, Huang Z, Krezel A, Zhao M, Tinberg CE, Lippard SJ, McNamara JO (2011) Vesicular zinc promotes presynaptic and inhibits postsynaptic long-term potentiation of mossy fiber-CA3 synapse. Neuron 71:1116–1126. CrossRef Medline

Paoletti P, Ascher P, Neyton J (1997) High-affinity zinc inhibition of NMDA NR1-NR2A receptors. J Neurosci 17:5711–5725. Medline

Paoletti P, Vergnano AM, Barbour B, Casado M (2009) Zinc at glutamatergic synapses. Neuroscience 158:126–136. CrossRef Medline

Qian J, Noebels JL (2005) Visualization of transmitter release with zinc fluorescence detection at the mouse hippocampal mossy fibre synapse. J Physiol 566:747–758. CrossRef Medline

Qian J, Noebels JL (2006) Exocytosis of vesicular zinc reveals persistent depression of neurotransmitter release during metabotropic glutamate receptor long-term depression at the hippocampal CA3-CA1 synapse. J Neurosci 26:6089–6095. CrossRef Medline

Ruiz A, Walker MC, Fabian-Fine R, Kullmann DM (2004) Endogenous zinc inhibits GABA(A) receptors in a hippocampal pathway. J Neurophysiol 91:1091–1096. Medline

Saadi RA, He K, Hartnett KA, Kandler K, Hershfinkel M, Aizenman E (2012) SNARE-dependent upregulation of potassium chloride co-transporter 2 activity after metabotropic zinc receptor activation in rat cortical neurons in vitro. Neuroscience 210:38–46. CrossRef Medline

Sedlacek M, Tipton PW, Brenowitz SD (2011) Sustained firing of cartwheel cells in the dorsal cochlear nucleus evokes endocannabinoid release and retrograde suppression of parallel fiber synapses. J Neurosci 31:15807–15817. CrossRef Medline

Sindreu C, Palmiter RD, Storm DR (2011) Zinc transporter ZnT-3 regulates presynaptic Erk1/2 signaling and hippocampus-dependent memory. Proc Natl Acad Sci U S A 108:3366–3370. CrossRef Medline

Tsien RW, Malinow R (1991) Changes in presynaptic function during longterm potentiation. Ann N Y Acad Sci 635:208–220. CrossRef Medline

Tzounopoulos T, Kraus N (2009) Learning to encode timing: mechanisms of plasticity in the auditory brainstem. Neuron 62:463–469. CrossRef Medline

Tzounopoulos T, Kim Y, Oertel D, Trussell LO (2004) Cell-specific, spike timing-dependent plasticities in the dorsal cochlear nucleus. Nat Neurosci 7:719–725. CrossRef Medline

Tzounopoulos T, Rubio ME, Keen JE, Trussell LO (2007) Coactivation of pre- and postsynaptic signaling mechanisms determines cell-specific spike-timing-dependent plasticity. Neuron 54:291–301. CrossRef Medline

Vallee BL (1988) Zinc: biochemistry, physiology, toxicology and clinical pathology. Biofactors 1:31–36. Medline

Varma N, Carlson GC, Ledent C, Alger BE (2001) Metabotropic glutamate receptors drive the endocannabinoid system in hippocampus. J Neurosci 21:RC188. Medline

Veran J, Kumar J, Pinheiro PS, Athan é A, Mayer ML, Perrais D, Mulle C (2012) Zinc potentiates GluK3 glutamate receptor function by stabilizing the ligand binding domain dimer interface. Neuron 76:565–578. CrossRef Medline

Vogt K, Mellor J, Tong G, Nicoll R (2000) The actions of synaptically released zinc at hippocampal mossy fiber synapses. Neuron 26:187–196. CrossRef Medline

Wilson RI, Nicoll RA (2001) Endogenous cannabinoids mediate retrograde signalling at hippocampal synapses. Nature 410:588–592. CrossRef Medline

Yasuda S, Miyazaki T, Munechika K, Yamashita M, Ikeda Y, Kamizono A (2007) Isolation of Zn^{2+} as an endogenous agonist of GPR39 from fetal bovine serum. J Recept Signal Transduct Res 27:235–246. CrossRef Medline

Zhang JV, Ren PG, Avsian-Kretchmer O, Luo CW, Rauch R, Klein C, Hsueh AJ (2005) Obestatin, a peptide encoded by the ghrelin gene, opposes ghrelin's effects on food intake. Science 310:996–999. CrossRef Medline

Zhang MY, Gao Y, Btesh J, Kagan N, Kerns E, Samad TA, Chanda PK (2010) Simultaneous determination of 2-arachidonoylglycerol, 1-arachidonoylglycerol and arachidonic acid in mouse brain tissue using liquid chromatography/tandem mass spectrometry. J Mass Spectrom 45:167–177. CrossRef Medline

Zhao Y, Tzounopoulos T (2011) Physiological activation of cholinergic inputs controls associative synaptic plasticity via modulation of endocannabinoid signaling. J Neurosci 31:3158–3168. CrossRef Medline

Zhao Y, Rubio ME, Tzounopoulos T (2009) Distinct functional and anatomical architecture of the endocannabinoid system in the auditory brainstem. J Neurophysiol 101:2434–2446. Medline

Zhao Y, Rubio M, Tzounopoulos T (2011) Mechanisms underlying inputspecific expression of endocannabinoid-mediated synaptic plasticity in the dorsal cochlear nucleus. Hear Res 279:67–73. CrossRef Medline

Zucker RS, Regehr WG (2002) Short-term synaptic plasticity. Annu Rev Physiol 64:355–405. CrossRef Medline